Planetary and Space Science 65 (2012) 38–57

Contents lists available at SciVerse ScienceDirect

Planetary and Space Science

journal homepage: www.elsevier.com/locate/pss

SPICAV IR acousto-optic spectrometer experiment on Venus Express

Oleg Korablev [a,b,*], Anna Fedorova [a,b], Jean-Loup Bertaux [c], A.V. Stepanov [d,a], A. Kiselev [a,b], Yu.K. Kalinnikov [d], A.Yu. Titov [e], F. Montmessin [b], J.P. Dubois [b,1], E. Villard [b,2], V. Sarago [b], D. Belyaev [a,b,c], A. Reberac [b], E. Neefs [f,g]

[a] Space Research Institute (IKI), 84/32 Profsoyuznaya, 117997 Moscow, Russia
[b] Moscow Institute of Physics and Technology (MIPT), 9 Institutsky dr., 141700 Dolgoprudny, Moscow Region, Russia
[c] LATMOS CNRS, Quartier des Garennes, 11 Boulevard D'Alembert, 78280 Guyancourt, France
[d] Faculty of Physics, Moscow State University, GSP-2, Leninskiye Gory, 119992 Moscow, Russia
[e] VNIIFTRI, 141570 Mendeleevo, Russia
[f] SKBKP IKI, 249810 Tarusa, Russia
[g] Belgian Institute for Space Aeronomy, 3 Av. Circulaire, B-1180 Brussels, Belgium

ARTICLE INFO

Article history:
Received 1 August 2011
Received in revised form
9 January 2012
Accepted 10 January 2012
Available online 13 February 2012

Keywords:
Venus
AOTF spectrometer
Spectroscopy

ABSTRACT

SPICAV IR, a part of SPICAV/SOIR suite on Venus Express, is a compact single pixel spectrometer for the spectral range of 0.65–1.7 μm based on acousto-optical tunable filter (AOTF) technology. SPICAV IR is derived from SPICAM IR operating on Mars Express, the first AOTF spectrometer in the deep space, and adapted for Venus atmosphere measurements. The spectrometer sequentially measures spectra of reflected solar radiation from Venus on the dayside and the emitted Venus radiation in spectral "windows" on the nightside, and works also in solar occultation mode. The spectral range is 0.65–1.1 μm with spectral resolution of 7.8 cm^{-1}, and 1–1.7 μm with spectral resolution of 5.2 cm^{-1}. A description of this near-IR instrument, its calibration, in-flight performances, and the modes of operations on Venus' orbit are presented. A brief overview of the science measurements is given: water vapor measurements in the mesosphere on the day-side and near surface on the nightside, mapping of the $O_2(a^1\Delta_g)$ emission at 1.27 μm, aerosol studies via polarization and scattering solar radiation at the day-side, and measurements of aerosol properties at the tops of the clouds in solar occultations.

1. Introduction

Venus Express is the first spacecraft sent to Venus after many years (Magellan operated till 1994). The science goals of the mission include the study of Venus' atmosphere, surface and environment from orbit observing remotely in the UV through IR spectral range, by means of radio science and in situ measurements of the ionized environment. Launched in November 2005, Venus Express arrived at Venus on 11 April 2006. After a series of orbit control maneuvers it reached the final operational 24-h orbit around Venus. The polar elliptical orbit now ranges between 66,000 and 250 km above the surface. The pericenter is located almost above the North Pole (80°N). To large extent its platform and its science payload has been inherited from Mars Express operating in the orbit around Mars from December 2003. The mission and operations are described in papers by Svedhem et al. (2007, 2009) and Titov et al. (2006).

Spectroscopy for the Investigation of the Characteristics of the Atmosphere of Venus/ Solar Occultation in the InfraRed (SPICAV/SOIR) is one of the seven experiments of Venus Express mission. The instrument consists of three independent spectral channels: ultraviolet grating spectrometer with an intensified CCD (118–320 nm, spectral resolution ~0.55 nm) SPICAV UV, near infrared acousto-optic (650–1700 nm, spectral resolution better than 1 nm) SPICAV IR, and infrared echelle-spectrometer with acousto-optic selection of diffraction orders SOIR for the spectral range of 2.2–4.3 μm (resolving power ~20,000). The instrument is dedicated to a number of studies of the Venus' atmosphere from the surface to the hydrogen corona (~40,000 km). The spectrometers can be operated in several observation modes, including nadir, limb and occultations for the vertical sounding of the atmosphere. The instrument is built by three organizations in France, Belgium, and Russia. Somewhat detailed description of the UV part of SPICAV/SOIR, primarily dedicated to stellar occultations and measurements

* Corresponding author at: Space Research Institute (IKI), 84/32 Profsoyuznaya, 117997 Moscow, Russian Federation.
E-mail address: korab@iki.rssi.ru (O. Korablev).
[1] Presently at Institut d'Astrophysique Spatiale, CNRS-Univ. Paris-Sud 11, 91405 Orsay, France.
[2] Presently at ESA ESAC P.O. Box, 78, E-28691 Villanueva de la Cañada, Madrid, Spain.

0032-0633/$ - see front matter © 2012 Elsevier Ltd. All rights reserved.
doi:10.1016/j.pss.2012.01.002

of SO_2 and SO above Venus clouds, and general issues related to other channels are discussed in paper by Bertaux et al. (2006, 2007a). The SOIR spectrometer dedicated to solar occultations to get vertical profiles of important minor constituents of Venusian atmosphere like CO, H_2O, HDO, HCl etc. is described by Nevejans et al. (2006), and its calibrations by Mahieux et al. (2008). Scientific results of SPICAV/SOIR are summarized in papers by Bertaux et al., 2007b; Vandaele et al., 2008; Fedorova et al., 2008; Marcq et al., 2011; Belyaev et al., 2008, 2012, and many others.

The present paper is dedicated to a somewhat detailed description of the SPICAV IR spectrometer, ground-based and in-flight calibrations and performance, various modes of observations, and an overview of the measurements on Venus. SPICAV IR is based on the design of SPICAM-IR channel on Mars-Express (Korablev et al., 2006, below as Paper 1) modified to adapt for Venus nightside observations. It is a pencil-beam spectrometer for the spectral range of 0.65–1.7 μm based on acousto-optical tunable filter (AOTF) technology integrated into the SPICAV/SOIR package. As well as the entire SPICAV/SOIR instrument, the AOTF spectrometer is a product of joint work of three institutions: Space Research Institute (IKI) in Moscow, Service d'Aéronomie du CNRS (now LATMOS/IPSL) in France, and Belgian Institute for Space Aeronomy. The spectrometer is developed and built in Russia, it is integrated into SPICAV and calibrated in France; some mechanical parts of SPICAV-IR and the solar port are fabricated in Belgium.

The spectrometer includes two channels, the short wavelength (SW) channel (0.65–1.1 μm) with spectral resolution of 7.8 cm^{-1}, and the long wavelength (LW) channel (1–1.7 μm) with spectral resolution of 5.2 cm^{-1}. Corresponding resolving power is superior to 1500. Both ranges are measured with two detectors, corresponding to two orthogonal polarizations. In terms of the spectral range this instrument complements on Venus Express the other channels of SPICAV/SOIR and Visible and Infrared Thermal Imaging Spectrometer (VIRTIS) (Drossart et al., 2007a), allowing somewhat better spectral resolution than VIRTIS-M channel. It is dedicated to dayside and nightside measurements in nadir, and profiling in solar occultations. Science goals of the experiment include measuring water vapor on the dayside, estimation of the cloud top altitude, and profiling of the aerosol and water vapor in occultation. On the night side it is dedicated to measuring of water vapor below clouds in the near IR transparency windows and atmospheric emissions. These measurements are addressed in detail below.

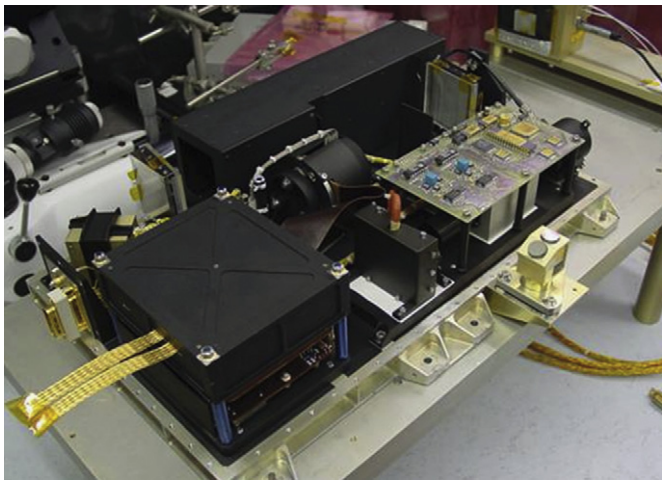

Fig. 1. SPICAV on a testbench without cover with the IR channel in front.

2. Instrument description

The first instrument employing the AOTF on a planetary space mission was SPICAM/Mars Express IR channel, described in detail in Paper 1 (see also Korablev et al., 2002a, b). On the Venus Express mission already two AOTF devices were included in SPICAV/SOIR package. One AOTF is used for the selection of diffraction orders in the echelle-spectrometer SOIR (Nevejans et al., 2006). The second, near-IR channel of SPICAV is the further development of SPICAM IR. For Venus studies, new requirements on spectral range, sensitivity, and dynamic range finally led to rather deep modifications of the instrument. The outlook of SPICAV IR AOTF spectrometer is shown in Fig. 1. Its main characteristics are summarized in Table 1.

2.1. The AOTF

Acousto-Optic Tunable Filter (AOTF) is a variable narrow band filter on the principle of Bragg's diffraction of light on the ultrasonic acoustic wave excited within a birefringent crystal. It can be electronically tuned to a desired wavelength using a radio frequency (RF) signal, typically below few watts applied to a piezoelectric transducer attached to the crystal. AOTF technology

Table 1
Characteristics of the SPICAV IR spectrometer.

Parameter	Short-wavelength range	Long-wavelength range
Spectral range	0.65–1.05 μm	1.05–1.7 μm
Spectral resolution	7.8 cm^{-1}	5.2 cm^{-1}
	0.42–1.44 nm	0.55–1.5 nm
	0.72 nm at 830 nm	0.9 nm at1300 nm
RF frequency range	250–140 MHz	140–80 MHz
FOV	2° circular (0.07° in Solar occultation)	
Telescope	Lens type, ∅12 mm; focal length 40 mm	
AOTF	TeO_2, Two actuators, Aperture 6×4 mm^2, 2°	
Detector	Two bicolor diodes (Hamamatsu K3413-05) 1 stage TE cooled to −15 °C	
	Silicon 2×2 mm^2	InGaAs ∅0.5 mm
NER (erg s^{-1} cm^{-2} sr^{-1} μm^{-1})	0.025	0.15
Gain control	8 gain values: 1–128 as powers of 2	
Time to measure one spectrum point T_M	1.4, 2.8, 5.6, 11.2, 22.4, 44.8, 89.6, 179.6 ms	
Dynamical range	2^{24}, packed into 2^{12}	
Data rate	6.2 kb per spectrum	
Power consumption	1.5 W average at 28 V	
Dimensions	$200 \times 85 \times 65$ mm^3 (not including DC/DC and DPU)	
Mass of the IR unit	700 g (not including DC/DC and DPU)	

is mature and the properties of such filters are extensively analyzed in the literature (see Paper 1 for references). AOTF suggests a light-weight and robust implementation of a spectrometer, potentially imaging, with a sequential spectral scanning.

Similarly to SPICAM/Mars Express, the AOTF of SPICAV is made of crystalline tellurium dioxide, TeO_2 in a specific non-collinear configuration (Epikhin et al., 1984), characterized by two orthogonal polarizations of the diffracted light. When the acoustic wave is not applied to the crystal, two undiffracted beams pass through, due to birefringence of the crystal (see Fig. 2). As soon as acoustic wave is applied, two diffracted beams deflected at $\pm 8^\circ$ appear. The strong undiffracted or "white" beams are captured by a light trap.

To cover the spectral range of 0.7–1.65 μm, the AOTF in the chosen configuration has to be operated in the frequency range of 80–250 MHz. Matching the acoustic and electrical impedances in such a broad range required a second, high-frequency actuator, to cover the part of the spectrum from 0.7 to 1–1.05 μm. The AOTF TeO_2 crystal is therefore equipped with two piezoelectric actuators. To avoid parallel sides in the crystal and parasitic standing waves, the high-frequency actuator is welded to the upper side of the crystal, and the acoustic wave reaches the active volume reflecting from the oblique side. In this range the filter operates in mode conversion regime: the longitudinal mode of the actuator converts into the slow shear wave for the acousto-optic interaction.

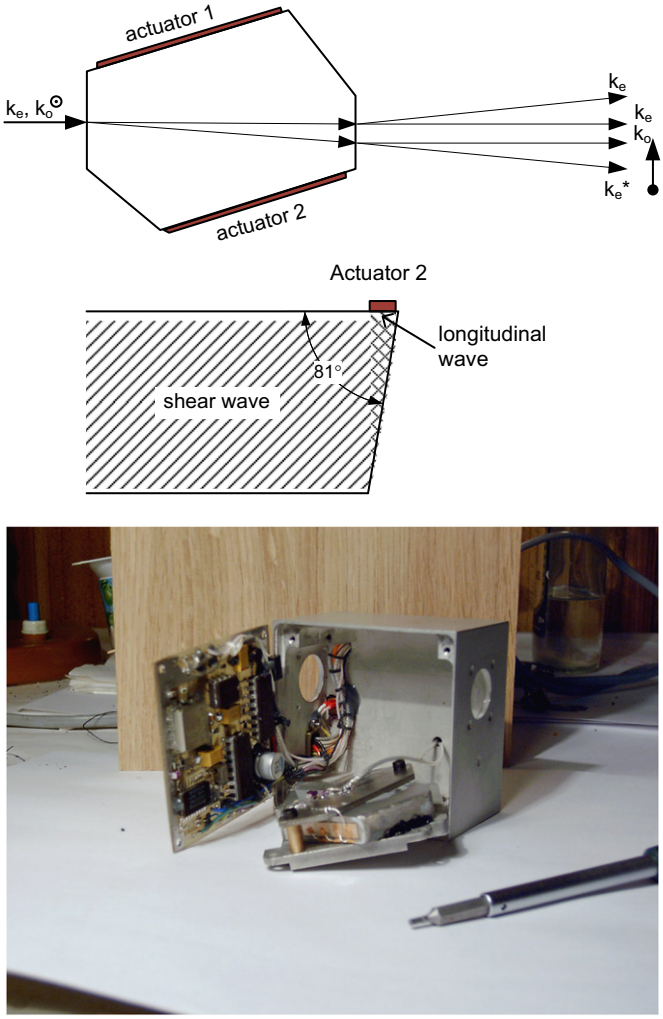

Fig. 2. The AOTF diagram and the inner view of the AOTF module with the acousto-optic cell in front.

Both actuators are 40 mm long. The length of the active zone (in which the acousto-optic interaction occurs) is ~25 mm. The input aperture is close to a circle with the diameter of 10 mm; the maximal angular aperture is $\pm 2.5^\circ$. Leaving the crystal the two orthogonally polarized beams can occupy the cross section up to 6×4 mm^2, and they are deflected at $\pm 8^\circ$. The deflection angle varies with the wavelengths from 7.6° at 1700 nm to 8.2° at 630 nm. The undiffracted zero order beams have the same 6×4 mm^2 cross section.

For the purpose of alignment, the spectral range of the short-wavelength channel attains the red line of HeNe laser line at 633 nm, but the AOTF efficiency at this extreme wavelength is low.

2.2. The optical scheme

The optical scheme of the AOTF IR spectrometer is shown in Fig. 3. The entry lens telescope collects the radiation from the planet. Its axis is parallel to all optical instruments on the spacecraft observing in nadir. For the Venus pencil-beam spectrometer, the narrow field-of-view (FOV) is of secondary importance, and we accepted the FOV of 2°, which allowed to simplify the entry telescope w.r.t. Mars Express version of the instrument. From the Venus Express orbit pericenter this FOV is equivalent to a track width of 9 km on the apparent surface of Venus. The telescope, doublet of TK14 and TBF10 lenses with the useful diameter of 12 mm and a focal ratio of 1:3.3 forms the image on a FOV diaphragm with the diameter of 1.1 mm.

To align the angular aperture of the AOTF crystal it is put into a collimator, which forms a pupil around the center of the acousto-optic zone. The AOTF collimator consists of smaller TBF10 lenses. The output lens (f=59 mm) serves to separate the "zero order" and the useful diffracted beams with orthogonal polarizations. Two symmetrically placed detectors with proximity lenses (Thorlabs A375, f=7.5 mm) are used for the ordinary and the extraordinary beams. To cover the wider spectral range and to increase the sensitivity at the visible side of the spectrum we used a combination of silicon and InGaAs, the so-called bicolor sandwich detector by Hamamatsu (K3413-05). The electrically cooled detector consists of a silicon 2×2 mm^2 photodiode on which is superimposed the InGaAs ∅0.5 mm photodiode. Two identical detectors with proximity lenses are used to analyze simultaneously the ordinary and extraordinary beams. The photodetectors can be cooled with the help of Peltier elements incorporated into their casings. They operate at 0.7 A current and typically provide the temperature 35° below ambient. There is no stabilization of the detector temperature.

The diffracted beams angles change by ~0.5°, as the device is tuned vary from 7.6° at 1700 nm to 8.2° at 630 nm. The surface of the silicon detector is excessively large making the angle variation unimportant for the SW channel. For the longer part of the spectrum, the drift is only ~0.2°, and after focusing it becomes insignificant, leaving the most of the radiation to reach the ∅0.5 mm photodiodes.

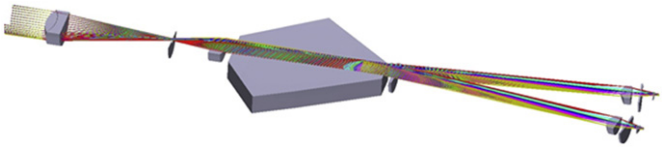

Fig. 3. The optical scheme of SPICAV IR. The elements are: telescope, FOV diaphragm, 1st collimating lens, AOTF, 2nd collimating lens, two detectors with proximity lenses. The detector's windows are shown. The inset shows rays hitting the InGaAs detector.

Generally, the improved sensitivity and long integration times during Venus nightside observations required special care about the stray light in the spectrometer, and dependable depletion of the "zero order" beam of the AOTF. Smaller InGaAs detector required more care about focusing of the output beams.

The SPICAV IR channel, similarly to the UV channel has the solar occultation sounding capability via dedicated solar port directed 90° from the axis of nadir-looking instruments. The solar light is collected with a small lens (useful diameter of 3 mm) forming the image on a circular diaphragm. When observing the Sun the angular FOV is about ∅4′. Then the solar light is fed into an optical fiber, which delivers it to the IR spectrometer. The pointing to the Sun is provided by the Venus Express spacecraft, providing on request the Sun orientation with an accuracy of better than 6′ (spacecraft specification). The solar port is normally closed by a shutter, which is opened only for the observation. There is no Sun detector.

SPICAV IR spectrometer is included in the UV package, but it is assembled on a dedicated baseplate. The AOTF cell and the RF electronics are mounted in a shielded unit with dimensions of $100\times60\times45$ mm^3 and a mass of 270 g. The telescope, the FOV diaphragm and the collimator are assembled in a tube-like rigid structure; the required precision is provided by mechanical tolerances. The telescope is attached to the AOTF unit. The light trap and the detectors with proximity lenses are mounted on the baseplate of the IR channel.

2.3. Measuring principle

The functional diagram of the instrument is presented in Fig. 4.

The intensities of diffracted IR beams are registered by two bicolor detectors (Si and InGaAs photodiodes). Typical sensitivity of the photodiodes is 0.5 A/W. When there is no acoustic activation of the AOTF (the RF is off) there is no diffracted light, and the instrument registers dark current of the photodiodes and some stray light inside the spectrometer. When the RF is on the photodiodes currents are the sum of dark current and photocurrent proportional to the intensity of incoming beam. Switching the RF on and off allows to measure the useful photodiode current: the difference of the two signals is calculated in the digital form. Each photodiode feeds current to low noise integrating preamplifier IVC102 (Texas Instruments and Burr-Brown) having 60 pF integrating capacitor. There are four preamplifier channels, following the number of sensitive elements: two for Si diodes and two for InGaAs. At the end of each measurement all integrators are zeroed simultaneously via common digital control line. The preamplifiers provide the gain of 10. The four output signals of preamplifiers along with other analog signals from various sensors are multiplexed to feed two following measurement channels. During the exposure either the pair of Si (SW range) or the pair of InGaAs (LW range) detectors is measured simultaneously. The proper pair of detectors is selected in accordance with the AOTF tuning range.

The two measurement channels provide programmable gain (1 or 4) and integrating amplifiers. In flight only the gain value of 4 was in use and the corresponding TC parameter (Boost) is assumed 4 hereafter (the exact multiplier equals 4.16). The gain of the integrating amplifier depends upon the integration time T_a chosen by a TC command. The resulting gain value approximately follows the expression $G=50\ \mu s/T_a$. The predetermined values of G are 1, 2, 4, 8, 16, 32, 64, and 128. Also, the integrating amplifier serves as a low-pass filter rejecting the high-frequency noise component. To fit into the ADC working range, a DC offset is added to the inverted signal from each of the measurement channels. The resulting relation between the input and output signals of variable gain amplifier is $U_{OUT}=K^*U_{IN}-2.5$ V, where K is the total gain of the amplifier. Both channels are feeding two 16-bit ADCs (ADS7813 from Texas Instruments) operating in ±3.3 V full-scale bipolar mode (32,768 negative and 32,768 positive grades; zero included).

The AOTF electronics comprises a programmable phase-lock RF synthesizer and a power amplifier. The two actuators of the AOTF are fed with two separate RF amplifiers, using common programmable RF synthesizer with f and $2f$ outputs. The power amplifier allows to control the output power, and therefore the AOTF diffraction efficiency. The corresponding TC parameter, DAC=3840, was chosen optimizing the AOTF efficiency against the power consumption, and remained unchanged for all ground

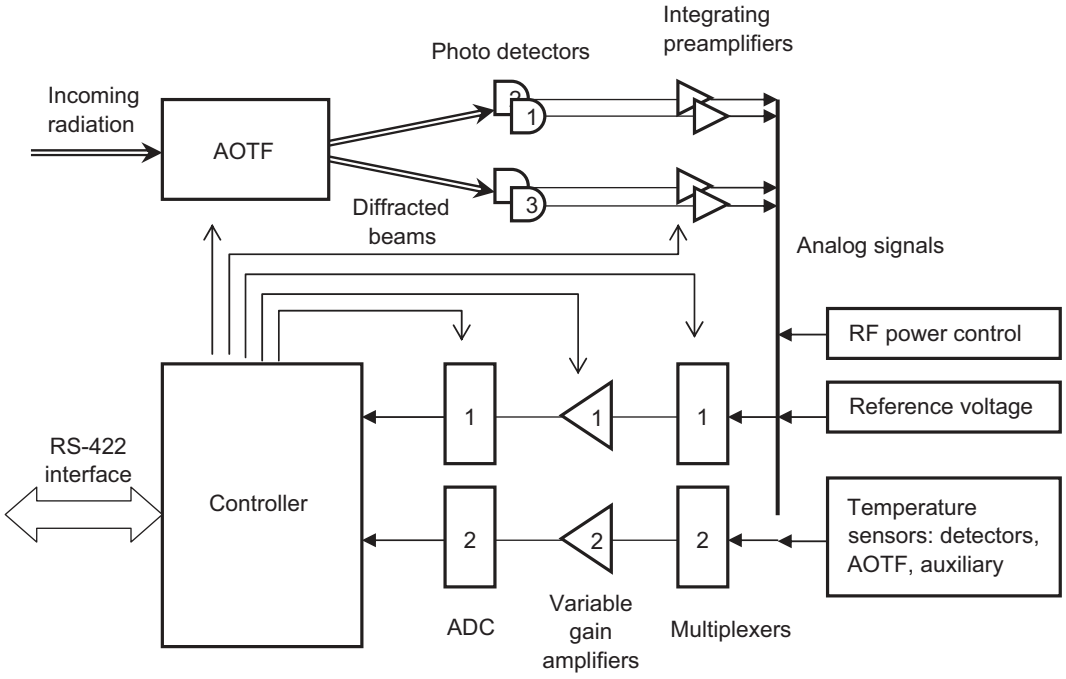

Fig. 4. Block diagram of SPICAV IR spectrometer.

and in-flight operations. The RF synthesizer and power amplifier are assembled in the AOTF unit that brings all RF into a shielded volume, minimizing electrical interference.

Overall measurement sequence is controlled and synchronized with 80c32 based controller operating at 30 MHz clock frequency incorporating 32K program ROM and 32K data RAM. The same controller supports the command and data RS-422 interface operating at 937.5 kbaud rate connected to the digital processing unit (DPU) of SPICAV. The registration and controlling system is assembled in a single block; the detector preamplifiers are located in the detector's proximity. The IR channel is powered from several ($+5$ V, ± 15 V, $+12$ V) secondary voltages provided by SPICAV-UV.

The time diagram of one SPICAV IR measurement is presented schematically in Fig. 5. At each measurement we measure the dark current (a combination of dark current and stray light), when AOTF is off and useful signal and calculate the difference. We employ the so-called correlated double sampling technique, well known from CCD applications, allowing to eliminate electronics offsets and the reset noise. The sequence is as follows: first, the AOTF frequency can be updated. At this moment the RF power is not applied to the AOTF transducer, and the useful optical signal at the output of the AOTF is zero (AOTF is off) letting the RF synthesizer ample time to settle the frequency. The instrument measures the dark current and the stray light, and two measurements ($D1$ and $D2$) are made at the beginning and at the end of the integration interval T_{INT}. In order to eliminate the electronic offsets the difference $D=D2-D1$ is calculated in digital form resulting in D value reflecting the dark current and the stray light current. Then the RF power is turned on, and two measurements of useful signals $S1$ and $S2$ are performed in the same manner. To reduce the high-frequency noise when reading the $D1$, $D2$, $S1$, and $S2$ values the signals are averaged using several ADC measurements at the beginning and at the end of integration period. It can be demonstrated that the optimal duration of the averaging is about one-third of the integration time, provided the integration time is long w.r.t. the noise correlation time. With the averaging the signal-to-noise ratio can be improved by a factor of $(T_{AVR}/T_C)^{1/2}$, where T_{AVR} and T_C are the averaging duration and the noise correlation time.

Additional unwanted effect of current/stray light background and offsets affects the dynamic range of the system. If these factors are large compared to useful photocurrent the accuracy of differential measurements is limited by digitalization, even if the noise is small. A typical offset voltage at the output of integrating preamplifiers is 2 mV, and dark currents of cooled photodiodes are about 3 pA for Si photodiode and 18 pA for InGaAs photodiode.

The difference $S=S2-S1$ is proportional to the sum of dark current, stray light and diffracted light. The difference $R=S-D$ is proportional to the intensity of the useful diffracted light only. The full time required to complete the above sequence, the sum of two equal integration times T_{int} and delays necessary for setting the frequency, data processing, etc., is the measurement time T_M. It can be programmed by software from 1.4 to 179.6 ms (1.4, 2.8, 5.6, 11.2, 22.4, 44.8, 89.6, and 179.6 ms integration times are possible). The above measurement procedure is applied to both measurement channels simultaneously, and sequentially to every point of the spectrum.

The overall amplification factor of the instrument and its sensitivity is determined by a non-trivial relation involving both G (the gain of the integrating preamplifier), and the spectral point measurement time T_M. The amplification factors calculated for different combination of T_M and G normalized to reference calibration mode

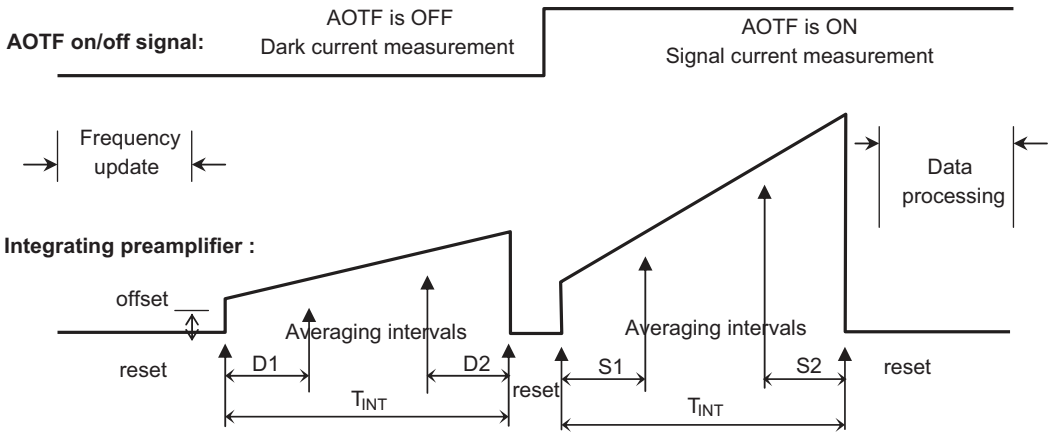

Fig. 5. The sequence of SPICAV IR elementary measurement.

Table 2
Overall amplification factor of SPICAV IR in function of measurement time (T_M) and preamplifier gain (G) parameters normalized to basic calibration mode ($T_M=2.8$ ms and $G=2$).

T_M	G							
	1	2	4	8	16	32	64	128
1.4	0.227337	0.39096	n/a	n/a	n/a	n/a	n/a	n/a
2.8	0.563713	1	2.31461	3.60981	n/a	n/a	n/a	n/a
5.6	1.23647	2.21808	3.41675	8.09193	17.4423	n/a	n/a	n/a
11.2	2.58197	4.65424	7.26966	17.0562	36.6292	75.7753	n/a	n/a
22.4	5.27298	9.52656	14.9755	34.9847	75.0031	155.04	315.113	n/a
44.8	12.4231	23.8269	43.5761	70.8417	151.751	313.569	637.205	1284.48
89.6	26.7234	52.4275	100.777	185.244	305.246	630.627	1281.39	2582.91
179.2	55.3241	109.629	215.18	414.049	762.856	1264.74	2569.76	5179.78

Table 3
Main modes of the SPICAV IR AOTF spectrometer employed on the orbit of Venus.

Mode	Objective	Sampling time (ms)	Window 1			Window 2			Window 3			Reference wavelengths	Duration of sp. (s)	Overall points
			λ_1 (nm)	λ_2 (nm)	Points	λ_1 (nm)	λ_2 (nm)	Points	λ_1 (nm)	λ_2 (nm)	Points			
Nadir 1 day	Full sp.	2.8	1040	1626	3320	692	1051	2656					17	5976
Nadir 2 day	Full sp.	5.6	1040	1626	3320	692	1051	2656					33	5976
Nadir 2 day	H_2O, CO_2	2.8	1246	1487	1243							Set 7	4	1328
Nadir 1 night	Full, BS	44.8	1040	1626	664	755	1051	664					59	1328
Nadir 2 night	Full, BS	89.6	1040	1626	664	755	1051	664					119	1328
Nadir 3 night	Full sp.	44.8	1040	1626	3320	791	1051	1660					223	4980
Nadir 4 night	Optimized	89.6	1046	1334	664	928	1051	332					89	996
Limb O_2	$O_2(a^1\Delta_g)$		1250	1287	110								10	110
Limb OH	OH		1408	1444	166								15	166
Star 1=Limb O_2	$O_2(a^1\Delta_g)$		1250	1287	110								10	110
Sun 1=Nadir 2	H_2O, CO_2,	2.8	1455	1465	22	1437	1330	546	1305	1284	61	Set 4	2	664

Note: Reference wavelengths are stored in the embedded software of SPICAV IR. In flight we used two sets of reference wavelengths:
Set 7: 14 wavelengths centered at 650, 760, 855, 980, 1101, 1160, 1198, 1242.6, 1274.6, 1305.7, 1324, 1515.4, 1553.6 and 1625 nm; 5 or 10 adjacent measurements for each reference wavelengths, in all 85 measurements.
Set 4: 11 wavelengths centered at 650, 760, 855, 980, 1101, 1160, 1198, 1274.6, 1324, 1553.6 and 1625 nm; 3 or 5 adjacent measurements for each reference wavelengths, in all 45 measurements.

(T_M=2.8 ms and G=2) are presented in Table 2. The reference mode was calibrated in flight as described in Section 3.3 below.

The ADC has the precision of 16 bit, all calculations are made with 24 bit accuracy, and the result of data processing is truncated to 16-bit words. To keep compatibility with SPICAV data blocks, allowing historically only 12 bit data, the 16-bit words are transformed into integer number in the form of $M \times 2^E$, where M is a 9-bit integer, and E is a 3-bit exponent.

2.4. Measuring modes

The frequency of the AOTF excitation is controlled by the software, allowing to access randomly any wavelength within the spectral range. To cover the complete spectral range with optimal sampling corresponding to the spectral resolution (2–3 points per resolution element) would require lengthy measurements often incompatible with observation scenario (in particular for limb or solar occultation measurements). For the atmospheric measurements one useful approach consists of measuring several "windows", containing the bands of atmospheric gases with optimal sampling, and a number of discrete spectral points (reference wavelengths) to characterize the spectral continuum (albedo of the clouds, reflectance at limb, extinction, etc.) through the full range of the instrument. This approach, validated for Mars (see Paper 1) allows to acquire up to three spectral windows, each characterized starting frequency, lengths and spectral step (sampling).

The observation modes of SPICAV IR, which are being considerably used in flight, are listed in Table 3. The corresponding observations are discussed in detail in Section 4. Although the device is programmed in frequencies, the table indicates the related (approximate) wavelengths (the wavelengths of the AOTF are temperature dependent, see below). Each measurement starts from the longest towards shorter wavelength; the device scans first the window 1, then windows 2 and 3 if needed. The measurement of the reference wavelengths is performed after completion of the window scan in the reversed order, i.e. from the shorter to the longer wavelength.

3. Ground and in-flight tests and calibrations

Before the delivery of SPICAV instruments to the prime contractor of Venus Express we have built one prototype and one "protoflight" unit of SPICAV IR. Later the spare flight model was completed. The shortened development cycle led to some lately discovered problems. The two-channel AOTF built first with transducers on parallel sides suffered from severe acoustic interference. This interference caused significant variation of the signal level in function of wavelengths, was also temperature dependent, making its calibration impractical. A new AOTF with conversion on the SW transducer (see Section 2.1) has been rapidly fabricated. This AOTF is now operational in the orbit around Venus. Unfortunately the LW channel of this final AOTF has revealed an anomaly, tentatively identified as a wedge irregularity in the transducer welding, the consequences of which are described in this section. The tight schedule of the Venus Express project did not allow further modifications, and this second AOTF was installed in the flight unit of SPICAV.

The laboratory calibration of the instrument was performed using several sources of continuous and discrete spectra: tungsten filament lamp, low-pressure pen-ray Xe, Ar, Hg–Ar lamps, He–Ne laser at 633 and 1152.3 nm. The most of laboratory measurements on the flight unit has been performed from 27 to 30 September 2004 after the replacement of the AOTF. Some examples of calibration spectra are presented in Figs. 6 and 7. The effectiveness in the LW cannel is significantly depressed w.r.t. the expected values and the SW channel, in particular in the middle of the spectral range (wavelength of ~1400 nm).

3.1. Dispersion curve and spectral response

To determine the wavelength assignment and the shape of instrumental function we used a number of laboratory sources of monochromatic light, such as Xe, Ar and Hg–Ne lamps and He–Ne laser at 633 and 1152 nm. The Xe, Ar and Hg–Ne lamps have several strong narrow lines that span representatively the spectral range of the spectrometer. For the LW channel the Hg lines at 1529.5, 1367.4, 1357.1, 1128,7 nm, Xe lines at 1473.2, 1262, 1083.8 nm, and Ar lines at 1350.4, 1295.67 nm were used. For the SW channel the Xe lines at 992.3, 980, 916.3, 881.9 nm, and Ar lines at 965.8, 912.3, 852.1, 826.65, 763.5 nm were used. The examples of measured spectra are shown in Fig. 6. The He–Ne laser was used to measure at 1152.3 and 632.78 nm lines. The shape of the instrument's spectral response function was determined with lines of HgAr, Ar and Xe low pressure lamps, which

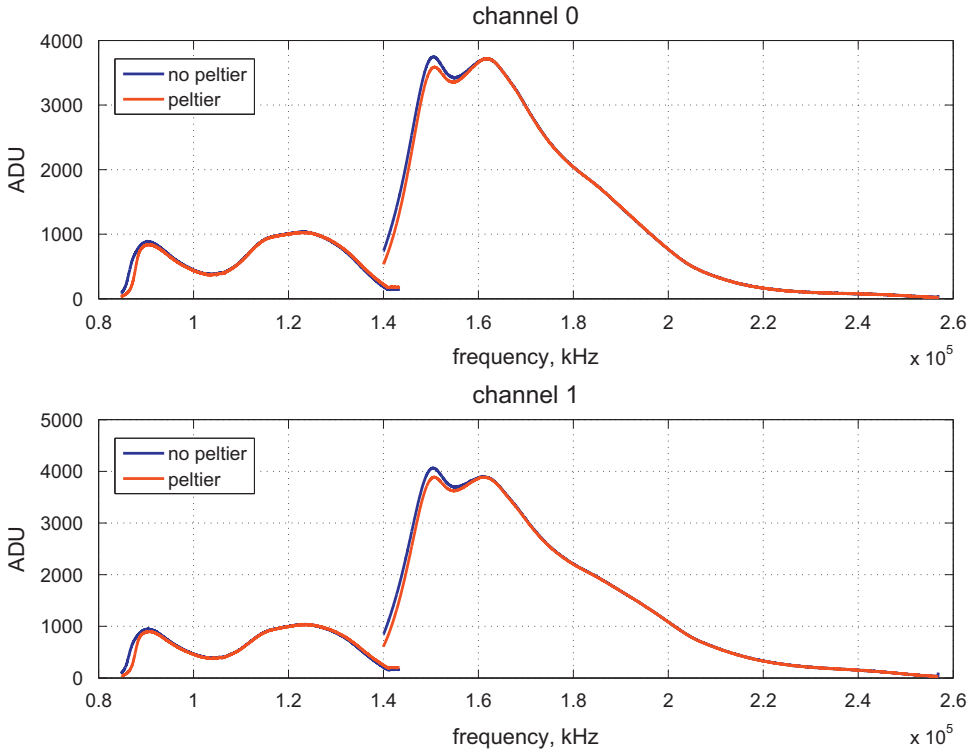

Fig. 6. Laboratory calibration of SPICAV IR with a source of continuum spectrum (filament lamp). The measurements have been performed for spectral point measurement time of 5.6 ms, $G=8$ at room temperature. The two curves correspond to cooled and uncooled detectors.

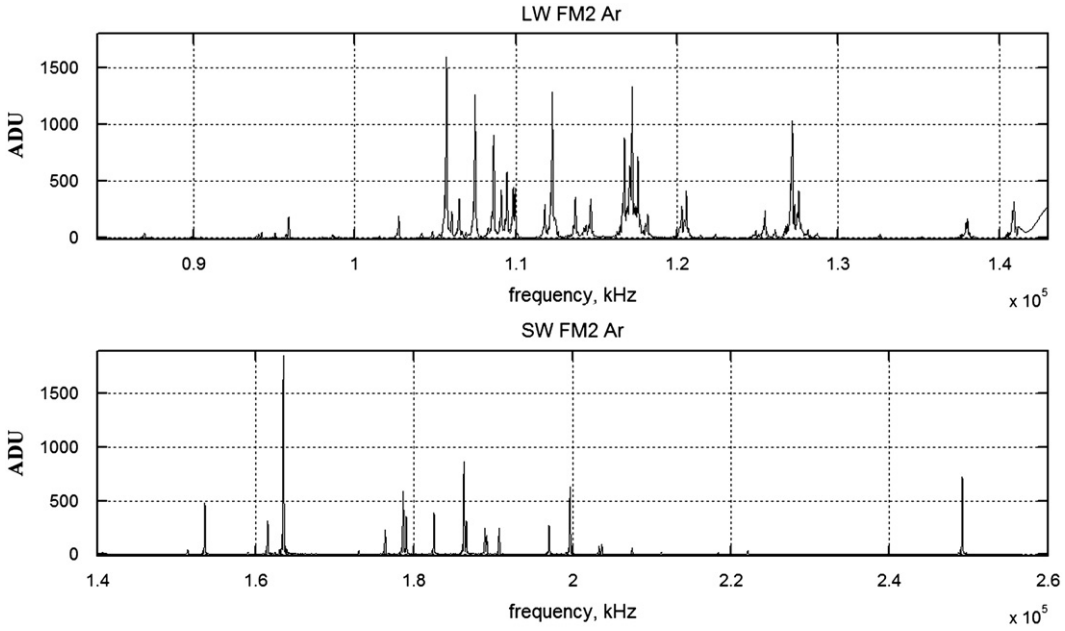

Fig. 7. Spectral calibration of SPICAV IR flight model using low pressure Ar lamp. LW channel is above and SW channel below.

can be considered as narrow (delta-function). Theoretically, the spectral response function of an AOTF is described as $(\sin x/x)^2$, and the spectral resolution, expressed in the AOTF frequency is approximately a constant within the spectral range. The spectral resolution in wavenumbers is modified with the dispersion of the TeO_2. We have accurately measured from several hundred runs the spectral response of the instrument for all the Xe, Hg and Ar lamp lines listed above. The spectral response of the AOTF for selected lines is presented in Fig. 8.

In the SW channel shape of the spectral response on the frequency scale is very similar for all the lines. The spectral response was measured using for both polarizations, and the difference is negligible. The full width at half maximum (FWHM) of the central lobe slightly decreases towards the longer wavelengths, less than for

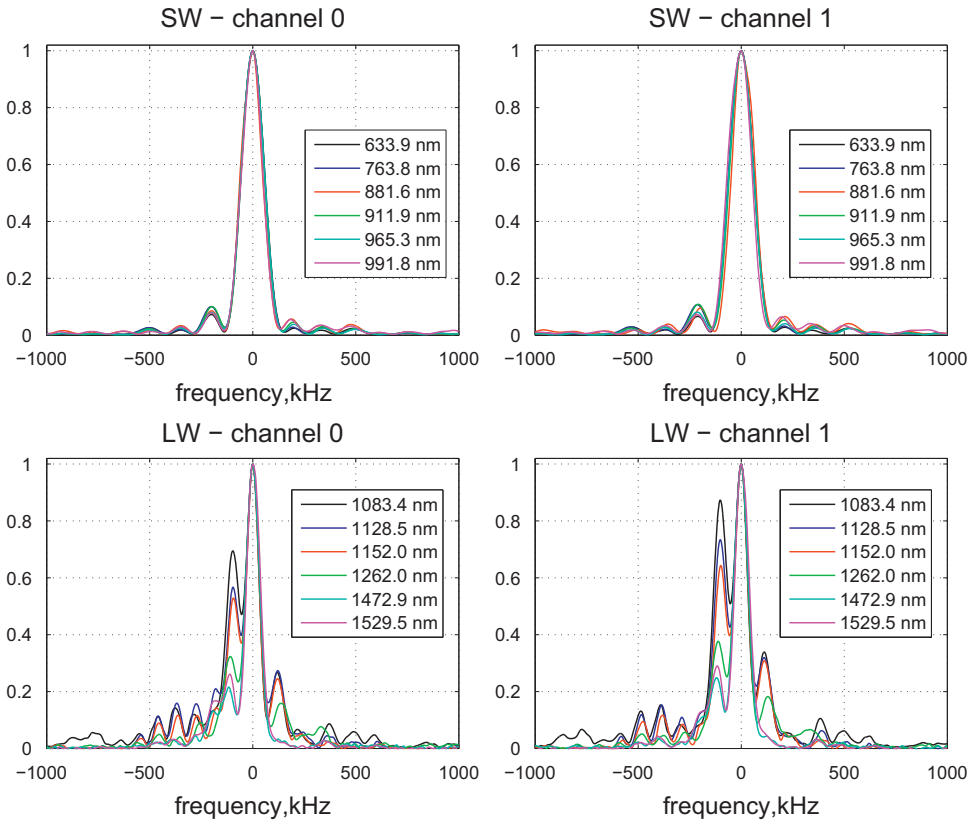

Fig. 8. Measured normalized spectral instrument function as a function of frequency for the SW (above) and LW (below) channels of SPICAV-IR. Theoretically the instrument function of an AOTF is described by $(\sin x/x)^2$.

10%. The side lobes are also very similar at different wavelengths. In contrast, the line profiles for the LW channel are not so uniform and the instrumental function has two maxima. This anomaly, and the depleted effectiveness, is likely connected with phase distortions in the ultrasound interface transducer-crystal, and is compatible with inhomogeneous welding of the transducer electrode (the wedge irregularity). The shape of the instrumental function significantly changes with frequency (or wavelength), and depends on polarization (it is different for the two detectors). We have also noted a little modification of the instrumental function after the launch (when analyzing the structure of the discrete $O_2^1\Delta_g$ band, see Section 4.2.4), but then it remained stable during 5-year operations. In addition to degradation of effective spectral resolution this complicated shape of the instrumental function distorts the appearance of the spectrum in LW channel and should be always taken into account when analyzing discrete LW spectra or searching for new lines.

The parameterization of the AOTF tuning curves is discussed in Paper 1. As previously, we used a simple but rather precise two-parameter parameterization that was enough for required accuracy of wavelength calibrations. The tuning curve of an AOTF can be described as $\lambda \sim a/f$, and in the units of wavenumber it can be approximated as

$$\nu = af^2 + bf + c \quad (1)$$

where the wavenumber ν is expressed in cm^{-1}, and the frequency f is in kHz.

The dispersion of the AOTF crystal changes with temperature, and the wavelength assignment of the AOTF spectrometer is expected to change with the drift of the crystal temperature owing to internal heat dissipation or environmental conditions (relative wavelength shift is $\sim 1.6 \times 10^{-2}$ nm K^{-1}). The AOTF unit is equipped with a sensitive temperature sensor in the proximity of the crystal. The laboratory measurements of the wavelength assignment were done at room temperature that is relevant for the measurements of the instrument function, but not enough to characterize the dispersion curve. The dispersion curve obtained in flight differs from ground calibrations, because of different temperature of the device. The typical temperature of SPICAV in-flight is around −10 °C varying from −21 °C to −4 °C. The wavelength assignment was then accurately measured in flight using ~20 solar lines, and controlled against positions of gaseous absorption features.

The calibration with solar lines for AOTF temperature of −10 °C was accepted as a reference. The temperature variations in-flight required shifts within 0.14 nm, introduced according to the positions of gaseous features. The resulting dispersion curves combining the laboratory and in-flight data for the SW and LW channels are presented in Fig. 9. The coefficients a, b, c of Eq. (1) for the in-flight calibration are listed in Table 4 for both channel and detectors. The dispersion is slightly different for two output polarizations of the AOTF (channels 0 and 1). The accuracy of this calibration is better than ±0.3 nm and ±0.5 nm within the LW and SW ranges, respectively, including the uncertainty due to the temperature shift.

As it was shown for SPICAM IR AOTF spectrometer (see Paper 1) the contribution of distant side lobes may be significant, e.g., side lobes with numbers higher than ±3 (the central lobe is 0) could contain up to 5% of the signal. For SPICAV IR the instrumental function was measured up to the 6th maxima on the each side, which are both below 0.1% of the maximal transmission. However, the exact impact of the distant side lobes is difficult to estimate from calibrations because of a number of potential systematic errors. The dependence of the FWHM of the central lobe on the wavelength is presented in Fig. 10. The resolving

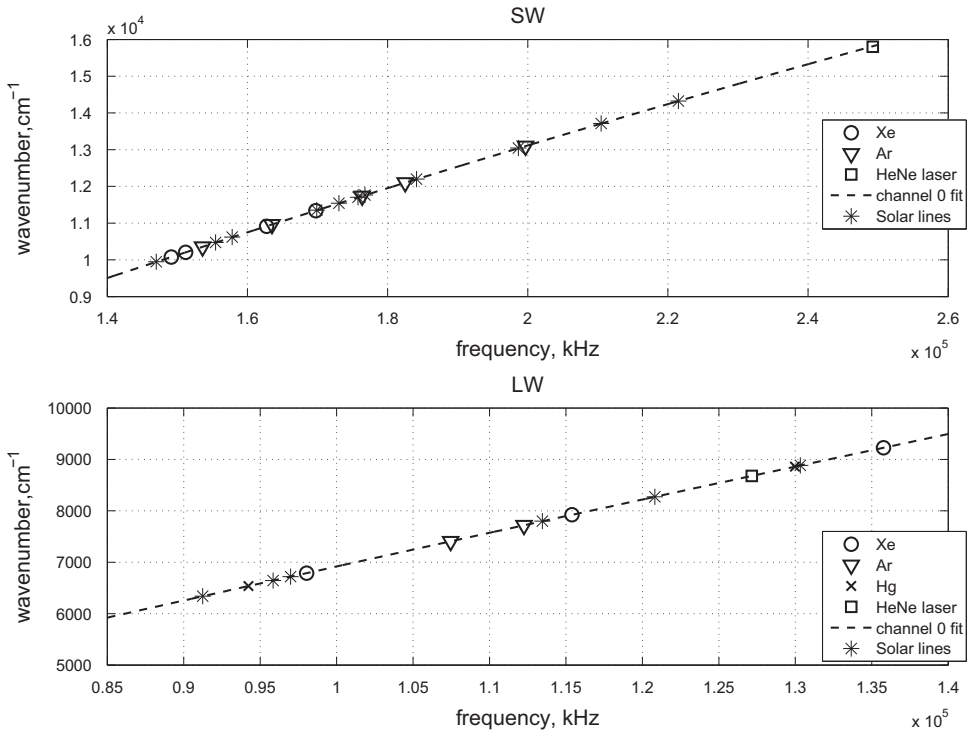

Fig. 9. The dispersion curves of SPICAV IR in function of the AOTF excitation frequency, according to solar lines, obtained in flight and lines of low pressure discharge lamps, obtained in the laboratory. All data are brought to the AOTF temperature of −10 °C. Fitting is made according to Eq. (1).

Table 4
Polynomial coefficients for the wavelengths calibration curve (Eq. (1)).

	a	*b*	*c*
Short wavelength channel (*SW*)			
Channel 0	−4.9405101e−008	7.6969006e−002	−2.9822051e+002
Channel 1	−5.0454785e−008	7.7358519e−002	−3.3244465e+002
Long wavelength channel (*LW*)			
Channel 0	−3.3865473e−008	7.2595705e−002	−2.0449838e+000
Channel 1	−3.5371703e−008	7.2919764e−002	−1.9140569e+001

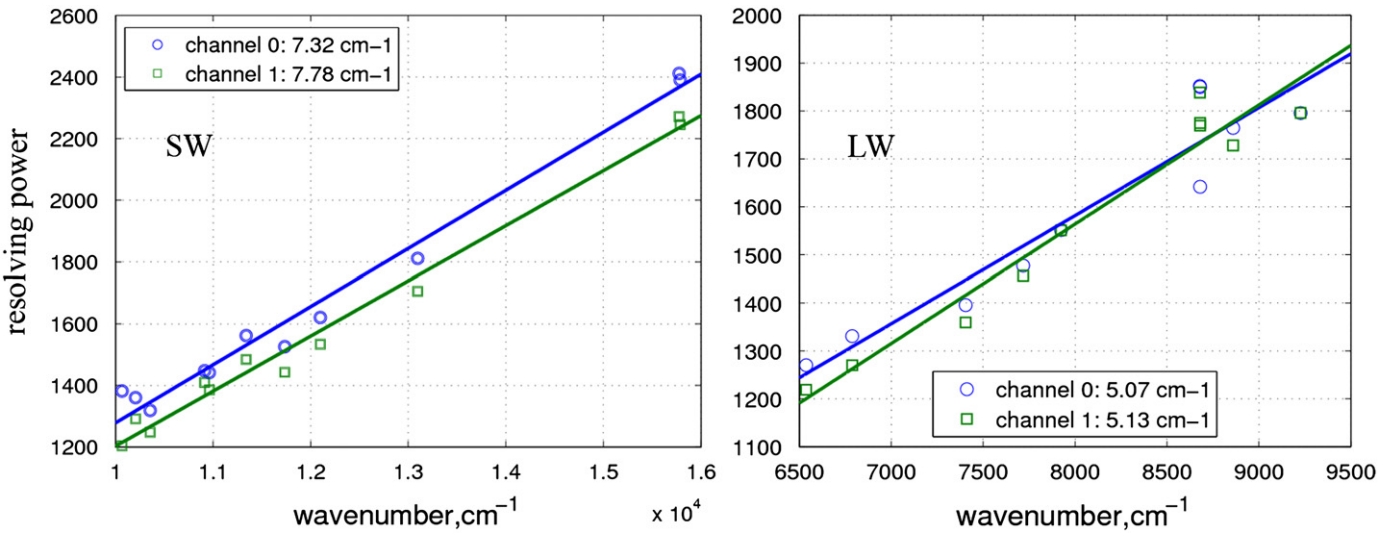

Fig. 10. Spectral resolution of SPICAV IR, as FWHM of the central lobe (see Fig. 8), in function of wavenumber (circles and squares—measured, solid—approximated by a straight line). Left panel: SW, right panel: LW range.

power $\lambda/\Delta\lambda$ of the instrument in the important spectral ranges of 1.38 μm and 0.9 μm amounts to 1400, and it is superior to 2000 at 1 μm for LW and 2400 at 0.65 μm for SW.

3.2. Dark signal (DC)

The measurements of the AOTF spectrometer are based on digital synchronous detection (see above), and for each measurement the dark signal is subtracted from the useful signal. Still, some background signal may propagate owing to synchronized optical or electrical interference. The synchronized RF interference from the AOTF driver was significant for the Mars version of the instrument (see Paper 1), forming a characteristic pattern in function of wavelength. For SPICAV the DC is much weaker but still it has to be taken into account during the data treatment especially for low signal. The cooling of the detectors substantially decreases the DC and noise and it is preferentially used in flight.

A special effort has been dedicated to characterize the background behavior in flight, as a function of particular observation modes, detector's temperature, integration time and gain. To support this study, the IR spectrometer was powered in the most practical observation regimes during several orbits when no significant signal in the IR was expected (e.g., while SPICAV UV observes in stellar occultations, away from the planet's disk). Fig. 11 shows the DC for typical nightside and dayside observation modes and for different gains. DC is significantly different for the two polarizations (Channels 0 and 1) owing to different electrical interference. In the SW channel the DC is lower, while in the LW channel it is more variable. The DC and its variations are especially important for the observations of weak signals on the nightside. For the dayside observations it can be considered insignificant both for LW and SW channels. For example, the derivation of the water vapor on the dayside is robust against the DC. On the other hand, a good knowledge of the background for both detectors is a must for polarization studies, which requires comparing absolute intensities that differ by less than 1–2%.

As soon as the background signal is determined, the correction procedure is trivial and consists of subtraction of the averaged smoothened background signal from each measured spectrum.

3.3. Absolute calibration, signal-to-noise, and polarization

The sensitivity calibration in the laboratory was to a band-shape filament tungsten lamp. The instrument response has been recorded for different integration times and gain values (Fig.6). The curves demonstrate also the sensitivity of the instrumental response to the cooling of the detectors, in particular near their long-wavelength cutoff (short frequencies), owing to photoelectric threshold.

The nominal temperature of the calibration lamp during the laboratory measurements was 2500 K. Approximated by the Planck function its spectral curve allows to estimate the sensitivity in absolute units ($W/m^2/\mu m/sr$). The laboratory measurements have been performed for a subset of integration times (T_M=2.8, 5.6, 11.2, 22.4 ms), and gain values (G=1…16), but not for sensitive modes with high gains and long integration times aimed for nightside observations (T_M=44.8 and 89.6 ms). The absolute dayside calibration was rectified in flight using Venus albedo data (Moroz, 1981).

We checked the absolute calibration of SPICAV IR in flight against the spectra measured by VIRTIS-M mapping spectrometer on Venus-Express (Drossart et al., 2007a; Cardesi´n et al., 2010). One VIRTIS-M pixel is only 0.25 mrad (0.86 arc min) against 2° FOV of SPICAV IR, in turn spectral sampling of VIRTIS-M is 13–17 nm in the near-IR against 0.9 nm for SPICAV. We compared SPICAV spectra convolved to VIRTIS spectral resolution with VIRTIS-M spectra integrated over the SPICAV IR FOV for a few orbits with relatively homogenous cloud albedo. The chosen orbit corresponds to typical day-side (T_M=2.8 ms and G=2) command of SPICAV IR used as the dayside reference. The examples of spectra are presented in Fig. 12a. Again, we noticed the modification of the sensitivity in the LW channel after the launch. It has further degraded (by a factor of ~0.6) in the vicinity of

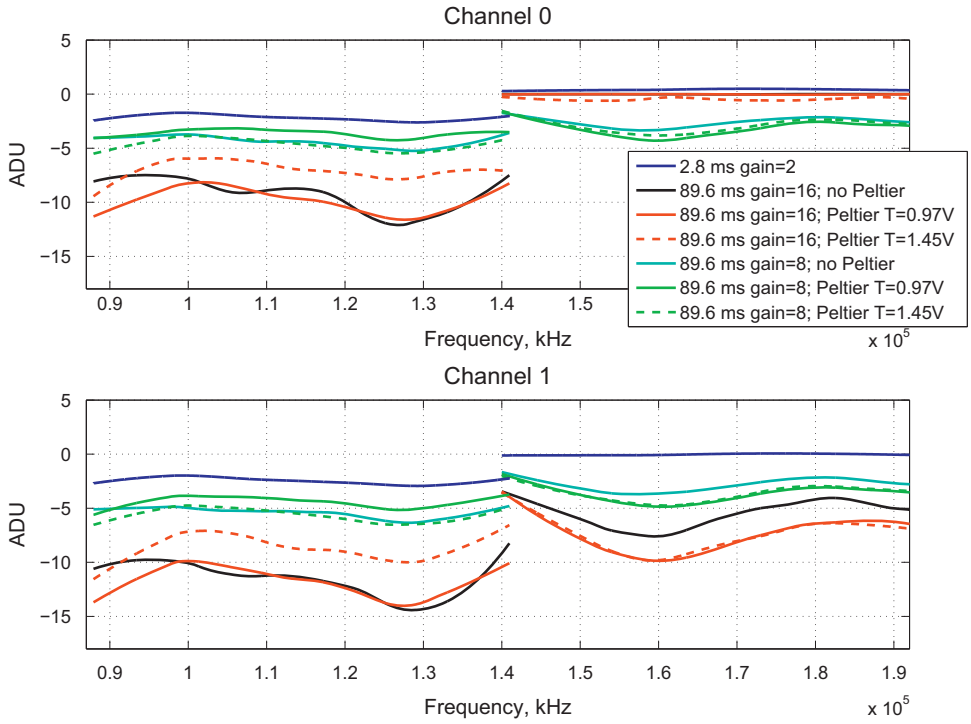

Fig. 11. DC of the instrument obtained in flight for different observation modes.

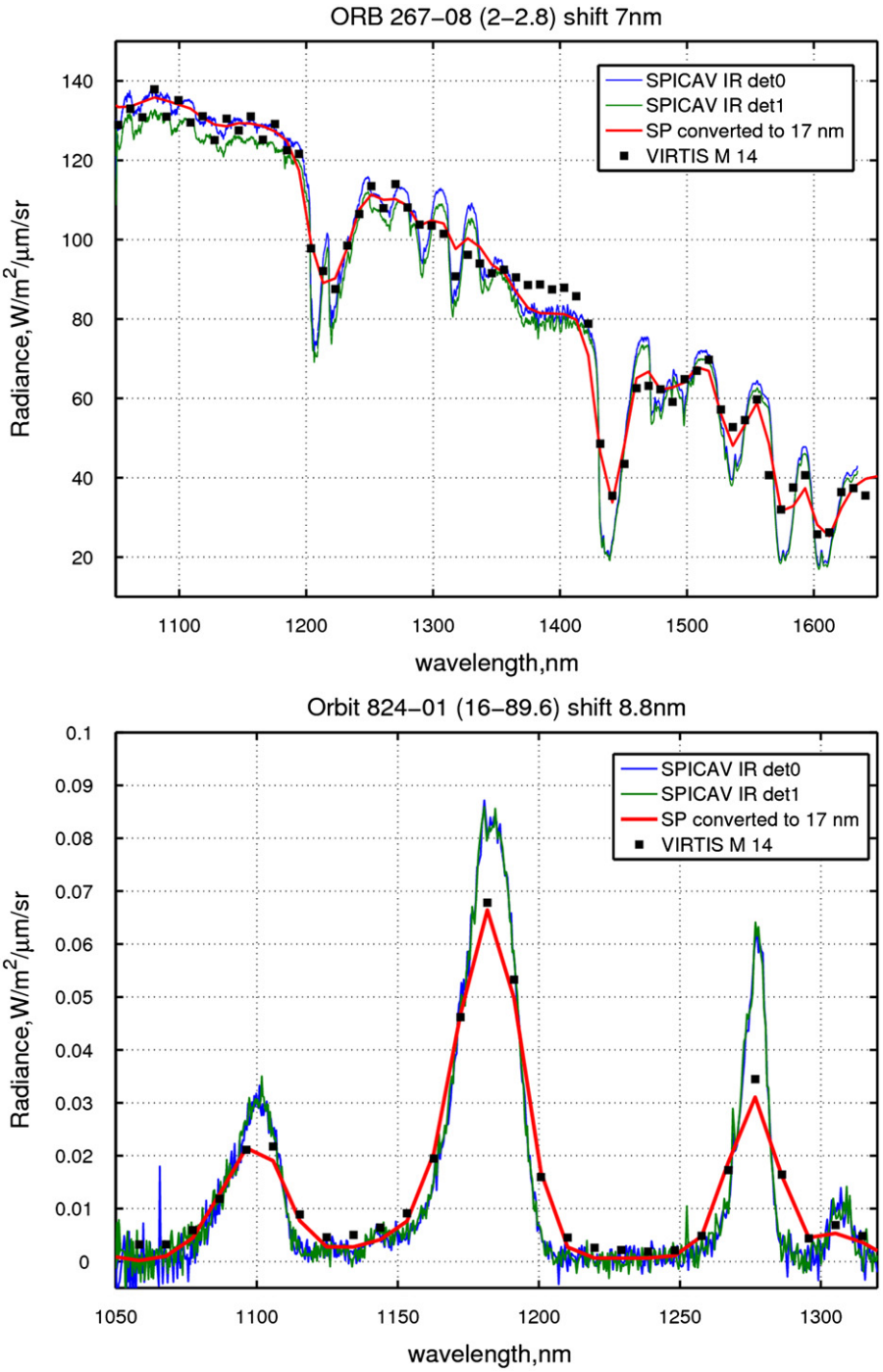

Fig. 12. Typical dayside and nightside spectra of Venus measured by SPICAV IR and compared to VIRTIS spectra. Top: Orbit 267 dayside (Latitude 30°S, Longitude 152°, SZA 56°, Spacecraft altitude 18000 km). Bottom: Orbit 824 nightside (Latitude 28°S, Longitude 261°, SZA 134°, Spacecraft altitude 51,000 km). SPICAV IR averaged for 15 spectra (blue and green curves) and converted to VIRTIS resolution (17 nm, Bézard et al., 2009) (red curve). In both cases VIRTIS M data for the same orbit have been averaged inside the SPICAV IR FOV (2°).

1300–1500 nm depletion, and remained stable for the whole duration of flight. We used VIRTIS data to correct the 1300–1500 nm range calibration.

The absolute calibration obtained for the reference observation command can be scaled to all other combination of T_M and G using the values from Table 2. The accuracy of Table 2 calculations can be illustrated by comparing nigthside SPICAV measurements (T_M=89.6 ms, G=16) with simultaneous VIRTIS-M observations (see Fig. 12b). We estimate the accuracy of the resulting absolute calibration as within 20% for all tested combinations of and G.

The noise-equivalent brightness (NEB) of SPICAV IR has been estimated from in-flight observations of the Sun and Venus. For the dayside observations (the best case) it reaches in the values of 0.05 and 0.5 W/m^2/μm/sr for SW and LW, respectively (Fig. 13). For long integration on the nightside this value is 0.0005 and 0.0025 W/m^2/μm/sr for SW and LW, respectively. The signal-to-noise is higher for SW (~3000) and low for LW channel (~100). As noted above, the effectiveness of the AOTF is depleted in the range of 1300–1500 nm, where the SNR is minimal (~60). This hampers the H_2O retrieval from 1.38 μm band. Presented is the

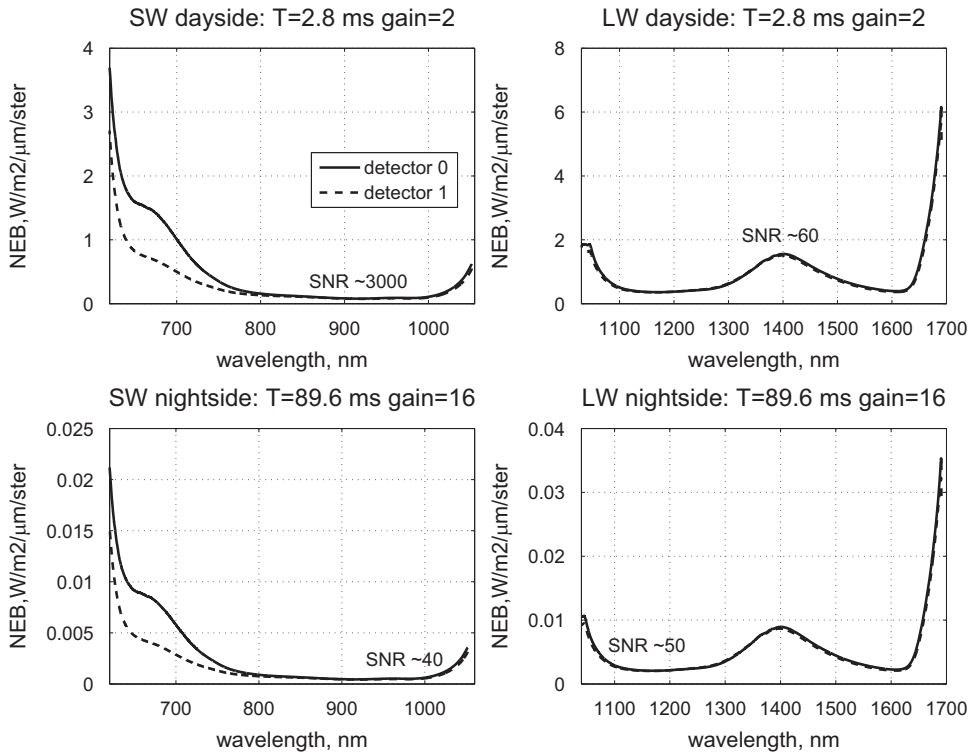

Fig. 13. The noise-equivalent-brightness (NEB) of SPICAV IR in the spectral range 0.65–1.7 μm for T_M=for 2.8 ms for the sunlight reflected from the Venusian clouds (top panels) and for T_M=89.6 ms for the nightside windows (bottom panels). The average signal-to-noise ratio (SNR) is indicated for some characteristic ranges. The NEB corresponds to cooled detectors.

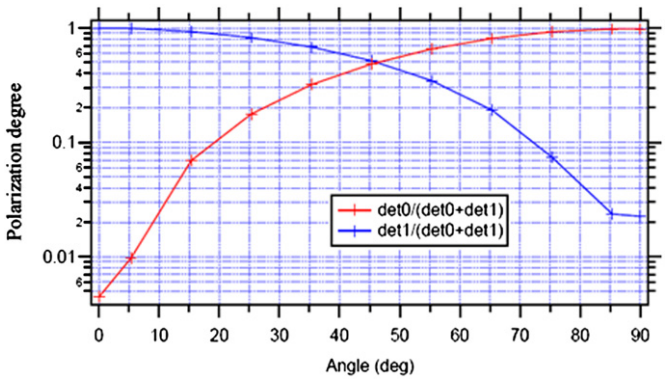

Fig. 14. Laboratory calibration: the signals from two channels of SPICAV IR are plotted as a function of the angle of a rotatable polarizer. The signals are normalized to the sum of both channels.

sensitivity of the instrument with cooled detectors. When the cooling is not applied, the NEB raises twofold.

Because of birefringent properties of TeO_2 crystal, the AOTF separates the incoming beam into two diffracted beams, which illuminate two detectors. The two beams are fully linearly polarized, with orthogonal directions. We have measured the polarization capabilities in the laboratory using the SPICAV IR spare flight model. These measurements are shown in Fig. 14 where the signals of both channels are plotted in function of the polarizer angle. The signals are normalized by the total flux, which is the sum of both channels.

The AOTF crystal inside SPICAV IR is oriented with respect to the spacecraft coordinates *X*, *Y*, *Z* (see Svedhem et al., 2007), with the polarization axes coinciding with *X* and *Z*. Nadir coincides with the *Y* direction. The nominal attitude of the spacecraft is "solar optimized", which means that the sun is kept always in the *XY* plane, and the solar panels are rotated around *Z* to maintain them perpendicular to the sun. Special efforts have been taken to provide additional calibrations of the polarization properties of the instrument in flight. To cross-calibrate the sensitivity of the two detectors we used opposition observations when phase angle (or solar zenith angle for nadir observations) equals zero, because in such case the polarization degree equals zero for symmetry reasons. This situation occurs every time when the orbital plane intersects the sun. The measurements have been performed for two orbits 464-01 and 1472 with the most complete coverage of the full spectral range 690–1640 nm. The measured ratio of signals in two polarization channels (detector 0/detector 1) has been used to correct the laboratory measurements.

4. Measurements

The IR channel of SPICAV has been operated from April 2006 simultaneously with the UV channel and SOIR. Up to June 2011 SPICAV IR has performed several thousand observations. The experiment in full measure uses the advantages of attitude control provided by Venus Express spacecraft. The main modes of observations include nadir, inertial limb, emission phase function (EPF) observations, solar and stellar occultations. These modes are very similar to Mars-Express operations as presented in Fig. 6 of Bertaux et al. (2006).

SPICAV IR operates as a point spectrometer with the FOV of ~2° and acquires wavelengths sequentially. As a result, each spectrum corresponds to a series of adjacent or overlapping spots positioned along the orbital ground or limb track. Different modes of observation imply different durations of spectrum scan following desired spectral range and sampling, different integration times, according to desired sensitivity and a number of auxiliary parameters (see Table 3). Mode names are arbitrary, and Nadir,

Limb, etc., designations indicate typical occurrences for each mode, according to its contents rather than a firm association with a particular observation mode of the spacecraft. The difference in the sensitivity of the IR spectrometer in Nadir mode, and in Sun observation mode is small due to much smaller aperture of the Sun port. During commissioning of the instrument we optimized the gain, and the IR spectrometer sensitivity is close to optimal at all the times. We will consider different modes one after another.

4.1. Nadir on the dayside

4.1.1. Operation modes

The high eccentricity of the Venus Express orbit allows to observe clouds and the atmosphere above clouds from the apocentre and to study higher northern latitudes in detail from the pericentre. The FOV of SPICAM IR (2°) corresponds to ~9 km from the Venus Express pericentre (250 km) and ~2000 km from the apocentre (66,000 km). A full scan of the spectral range at fine spectral sampling (1–2 points per element of the spectral resolution) requires 3320 points in the LW of SPICAV IR and 2656 points in the SW range. The clouds reflect about 70% of solar flux and the Venus is very bright in visible and near-IR spectral range, allowing to reduce the integration time to 2.8 ms (typical integration time on Mars is 5.6 ms). Full spectrum requires then 17 s to be measured (command "Nadir 1 day"). From the apocentre the ground speed amounts to 0.12 km/s, and the monochromatic spot in nadir is nearly circular because the measurement of one spectral point is almost instantaneous. The extent of the full spectral record on the ground is approximately 2000×2010 km, justifying this mode for the apocentre observations.

In the pericentre the ground speed is very fast (~10 km/s) and it is therefore desirable to keep the time to measure one spectrum as low as possible. We therefore restricted the measured ranges to the most interesting parts, defining parameters of the "windows" as described in Section 2.4). The mode Nadir 3 day, which is mostly used for near-pericentre observations consists of one window. The spectral range of 1246–1487 nm is acquired at somewhat loose sampling and characterizes features of CO_2 and H_2O gases. A number of reference wavelengths from 650 to 1625 nm (see Table 3) allow to characterize the rest of the continuum. The command contains 1328 points. As a result, we obtain one spectrum per 4 s (the extent of the spectral record on the ground of 10×40 km^2) (see Table 3).

4.1.2. Cloud top and H_2O measurements

Atmospheric water is one of important gases on Venus. The question why Venus is so much drier than the Earth is crucial to understanding the evolution of the Venus atmosphere. H_2O plays a significant role in the chemistry of the lower and middle atmosphere of Venus being involved in the sulfur oxidation cycle that produces H_2SO_4, and in active photochemistry above the clouds. Water vapor abundance was constrained by several space experiments and ground-based observations. The H_2O abundance above clouds has been measured by Pioneer Venus Orbiter Infrared Radiometer and Venera 15 Fourier Transform Spectrometer (Koukouli et al., 2005; Ignatiev et al., 1999). The PV OIR measurements demonstrated substantial variations of H_2O abundance in the equatorial region shortly after the sub-solar point. The variations of water vapor in the mesosphere have been also reported by ground-based in microwave observations (Sandor and Clancy, 2005). Venus Express experiments offered the first long-term monitoring of H_2O in the Venusian mesosphere during several years. VIRTIS-H measures H_2O in the 2.56 μm band (Cottini et al., 2012). SOIR provides vertical profiles of H_2O in the 2.56 μm band in the altitude range from 70 to 110 km (Bertaux et al., 2007b; Fedorova et al., 2008). SPICAV IR measurements in the 1.13 and 1.37-μm bands are sensitive to water vapor contents near the cloud tops somewhere above the effective sounding altitude of VIRTIS and below the lowest altitude of SOIR profiles. Together the three spectrometers help to construct a complete 3D map of H_2O above the clouds.

A typical spectrum measured by SPICAV IR in nadir near the apocenter for an early Orbit 30 is presented in Fig. 15. The main features of the spectrum are the spectral slope towards the longer wavelengths, a number of Fraunhofer solar lines especially in the SW channel, and some atmospheric absorption features, the most prominent being CO_2 bands at 1.2, 1.22, 1.3, 1.43, 1.58, and 1.6 μm, and H_2O bands around 1.13 and 1.37 μm.

To construct a synthetic model relevant to the observed spectrum we have to account for gaseous atmospheric absorption by CO_2 and H_2O, cloud vertical distribution and the solar spectrum. Gaseous absorption is computed line-by-line using the spectroscopic database HITRAN-2008 (Rothman et al., 2009). Temperature and pressure profiles are taken from the VIRA model (Keating et al., 1985). The vertical distribution of water in the atmosphere is assumed uniformly mixed above the clouds with mixing ratio of 5 ppm. Aerosol properties are assumed from Venera 11–14 data (Ignatiev et al., 1997) with $\tau=1$ at 60 km. An important issue is the accurate solar spectrum, because numerous solar lines mix up with the signatures of atmospheric gases. There are few sources of high-resolution solar spectrum in spectral range of interest. A theoretical spectrum by Kurucz et al. (1995) and the SOLSPEC spectrum (Thuillier et al., 2003) are at the limit of the required spectral resolution. The presented model implies SOLSPEC data, revealing some disagreements with solar features in SPICAV spectra.

Fig. 16 shows the portion of a pericentre spectrum centered on the H_2O–CO_2 range. The absorption in the carbon dioxide bands allows to measure the cloud top altitude basing on their equivalent width or relative depth. On Venus Express this method was already employed to retrieve the cloud altimetry with VIRTIS-M mapping spectrometer from the 1.6-μm CO_2 band (Ignatiev et al., 2009). Knowing the altitude of clouds the water contents above them can be retrieved from the absorption band at 1.37 μm. The band is reasonably well resolved, and the retrieval is possible even if the shape of the spectrum in this range is modified with uneven spectral continuum. An iterative process allowing to fit both the smooth continuum, and the water vapor contents is described by Fedorova et al. (2006) for the case of Mars. The multiple scattering in the clouds has been modeled using the SHDOM code (Evans et al., 1998). To accelerate retrieval computations, the absorption in the H_2O 1.38 μm band was tabulated in function of the solar zenith angle (SZA), H_2O contents, atmospheric scale height, and cloud altitude at $\tau=1$. The details of the retrieval procedure, and the resulting mapping of the atmospheric water by SPICAV (from April 2006 to November 2010) can be found in paper by Fedorova et al. (2010).

4.1.3. Polarization measurements

Polarimetry observations have long remained the only source of information constraining the properties of the particles in the Venus clouds. From the orbit around Venus Photopolarimeter experiment aboard Pioneer Venus provided polarization measurements from UV (270 nm) to near infrared (935 nm). Explored by Kawabata et al. (1980) and Sato et al. (1996), these data pointed to small (~0.25 μm) droplets of H_2SO_4 at 85% concentration as most probable candidates for cloud particles.

SPICAV IR on Venus Express offers polarization as a tool of diagnostic for the particle size and composition. Observing the solar light scattered by ground and aerosols in nadir, the AOTF spectrophotometer records the intensity and the polarization as a function of wavelength. Because of birefringent properties of the

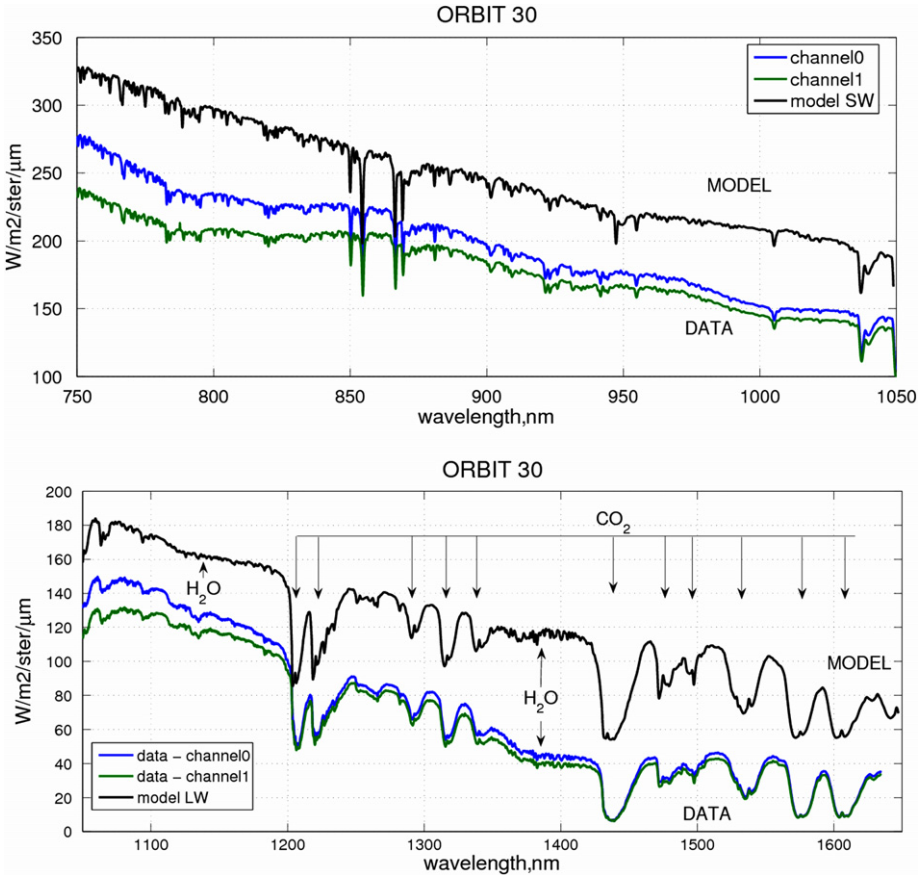

Fig. 15. An example of SPICAV IR spectrum recorded during orbit 30 (latitude −58°, longitude 160°, SZA 64°). 15 spectra have been average. The synthetic spectrum includes solar spectrum, CO_2 and H_2O absorptions and the cloud model (see text). Assumed H_2O mixing ratio equals 5 ppm. The model spectrum is shifted by 50 W/m^2/µm/sr to simplify the comparison.

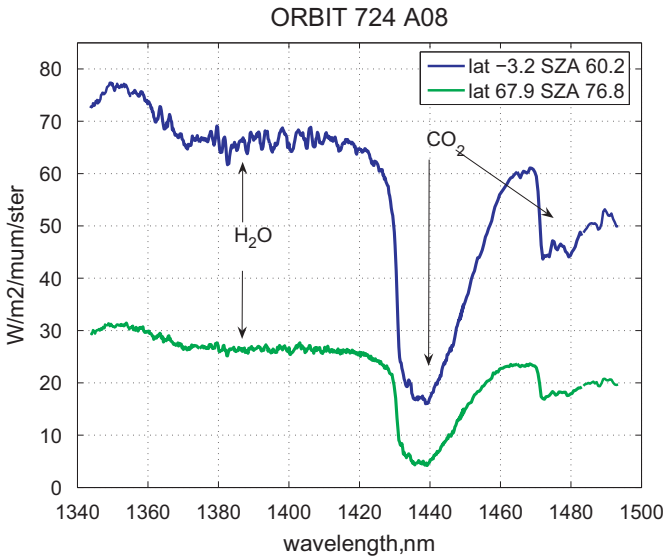

Fig. 16. Example of "Nadir 3 day" observations at orbit 724 near the pericenter. CO_2 and H_2O bands are presented.

AOTF its two output beams are fully linearly polarized, with orthogonal directions (see Sections 2.1 and 3.3). Therefore, the degree of polarization, *P* is recorded in addition to the total flux for each nadir measurement, for all wavelengths defined by the chosen measurement mode. Variations of *P* with the phase angle, which in nadir equals to the local SZA may be obtained on a statistical basis. Measurements at the reference wavelengths allow to determine the variation of reflectance and polarization with wavelength, which are strongly dependent on the cloud particle properties in the full range of SPICAV IR (650–1625 nm, see Table 3). A scattered plot of the polarization degree at an example wavelength 1159.7 nm for all nadir orbits from 23 to 1200 is shown in Fig. 17.

4.2. Nadir and limb at night side

4.2.1. Operation modes

The nightside observations require high instrument sensitivity. The integration times used are 44.8 and 88.9 ms increasing the time to measure one spectrum of 4980 points up to 2.5 min. Under-sampling (e.g. full spectrum of 1328 points) decreases the measurement time, but narrow features may escape detection. The relevant commands are listed in Table 3 as "Nadir 1–3 night". These modes are used for general survey and calibration purposes. Science observations were performed in nightside "spectral windows": 928–1051 nm for SW and 1046–1333 nm for LW. The mode "Nadir 4 night" contains 996 points and requires about 1.5 min. This mode is mostly used for the nightside apocentre observations.

Limb observations are short, and lengthy modes are not acceptable. In 1.5 min the line of sight typically traverses the entire limb precluding any meaningful measurements. To achieve some vertical resolution shorter sequences are necessary. The limb observations first targeted the detection of atmospheric emissions. The command "Limb O2" aimed to characterize the

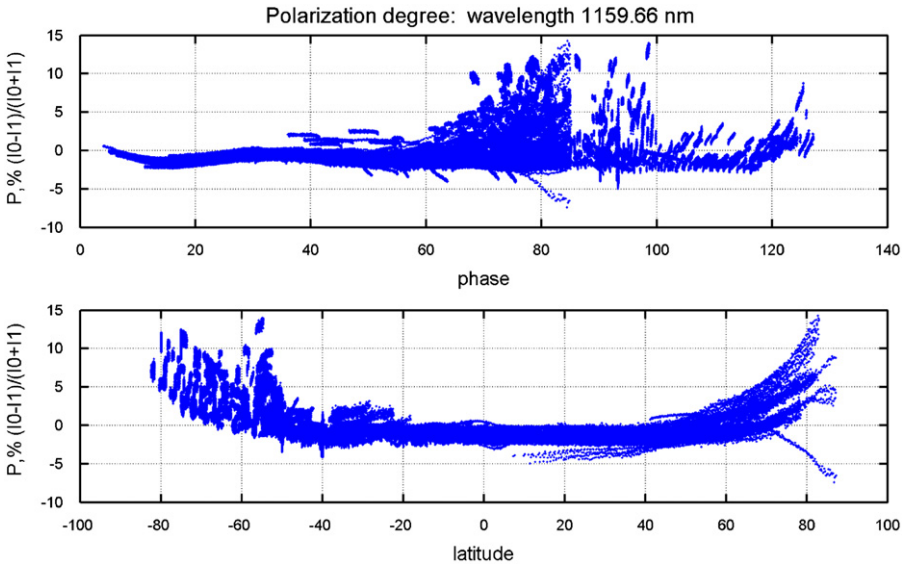

Fig. 17. Polarization degree of the light reflected at Venus cloud top measured by SPICAV IR at an wavelength of 1159.7 nm for all orbits from 23 to 1200 in function of phase angle and latitude.

O_2 emission on limb. It takes 10 s and contains 110 spectral points in the range of 1250–1287 nm. The command "Limb OH" allows to measure 166 points in the range of 1408–1444 nm in 15 s. The sensitivity of the instrument is insufficient to detect any starlight in the IR, but the channel is routinely turned on in "Limb O2" or "Limb OH" modes to search for emissions on Venus during the stellar occultations, which are observed in the UV.

4.2.2. Nightside windows

The "nightside windows" are night IR emissions originating from hot deep atmosphere and the surface in spectral ranges located between the strong absorptions by CO_2 and water vapor. Since their discovery by Allen and Crawford (1984), the windows have been repeatedly explored by ground-based observations (Crisp et al., 1991; Bézard et al., 1990; Meadows and Crisp, 1996) and fly-by spacecraft (Drossart et al., 1993; Baines et al., 2000). The brightest windows are located at 1.74 and 2.3 μm; other windows are at 0.85, 0.9, 1.10, 1.01, 1.18, 1.27 and 1.31 μm (Crisp et al., 1991). In the shorter wavelength windows, 0.85–1.01 μm, the atmosphere is optically thin, and virtually all the radiation observed from space originates from the surface. This makes possible mapping the surface temperature and/or emissivity (Baines et al., 2000; Hashimoto and Sugita, 2003). In the longer wavelength windows, 1.31, 1.74 and 2.3 μm, the radiation originates from different levels of the atmosphere. The windows have been extensively used to probe the chemistry of the deep atmosphere, especially the complex window at 2.25–2.50 μm indicative to minor constituents CO, OCS, H_2O and SO_2 (e.g. Pollack et al., 1993; Tsang et al., 2008; Marcq et al., 2008). Recently discovered 1.51 and 1.55 μm windows have been analyzed and modeled by Wilson et al. (2009).

The spectral range of SPICAV IR (0.65–1.65 μm) includes the windows 0.85, 0.9, 1.01, 1.10, 1.18, 1.27, 1.31, 1.51 and 1.55 μm. An example of SPICAV IR nightside spectrum measured on the orbit 34 (11 spectra averaged) is shown in Fig. 18. In the SW range all the three windows 0.85, 0.9, and 1.01 μm are well detected. In the LW range, the windows 1.10, 1.18, and 1.27 μm are prominent, 1.31 μm is well detected. Noticeable is the narrow peak of $O_2^1\Delta_g$ emission within the 1.27-μm window. Much weaker 1.51 and 1.55 μm would require larger averaging. Typically one orbit contains 15–20 spectra. The SPICAV provides track measurements of night windows with relatively high spectral resolution complementing simultaneous observations of VIRTIS-M with low spectral resolution but mapping capability and higher signal-to-noise (Wilson et al., 2009; Bézard et al., 2009, etc.) After the malfunction of VIRTIS-M SPICAV IR remains the only instrument covering this short wavelength IR range on Venus Express.

4.2.3. H_2O measurements

The 1.10 and 1.18-μm windows are limited from one side by the $\nu_1+\nu_2+\nu_3H_2O$ band centered at 1.13 μm and on the other side by CO_2 bands ($2\nu_1+3\nu_3$ band at 1.05 μm and $\nu_1+3\nu_3$ band at 1.21 μm). Imaging and spectroscopic observations in these windows can therefore provide information on the water vapor abundance and its variations near the surface. Ground-based observations of Venus' night side in the 1.18-μm window established H_2O mole fraction of 30 ± 10 ppm (Crisp et al., 1991; Pollack et al., 1993). From spectro-imaging data covering a broad range of surface elevations, Meadows and Crisp (1996) derived a slightly larger H_2O mole fraction, 45 ± 10 ppm. From spectral data of Venera 11, 13 and 14 descent probes Ignatiev et al. (1997) concluded that the H_2O mixing ratio is between 20 and 40 ppm in the altitude range 5–60 km. Below 5 km, the quality of the Venera data is depleted but an increase of the H_2O mixing ratio up to 50–70 ppm towards the surface was suspected. These results demonstrate significant uncertainties remaining among water measurements near the surface. In particular, spectral analysis in the near-infrared windows is hampered by poor knowledge of the CO_2 continuum opacity at high pressures, high temperatures, and long path lengths, arising from collision-induced bands and extreme far wings of allowed CO_2 bands.

Only limited information about horizontal or temporal variations of water near the surface is available to date. Horizontal variations of the H_2O abundance were searched by Drossart et al. (1993) using Galileo/NIMS data in the 1.18-μm window. Over a limited area covered they found the variations inferior to 20% in the altitude range of 0–15 km. Analyzing VIRTIS-M data Bézard et al. (2009) retrieved water vapor mole fraction of 44 ± 9 ppm in the southern hemisphere with stringent upper limit for latitudinal variations: $\pm1.5\%$ in the range 60°S–25°N and $\pm3\%$ for a broader range of 80°S–25°N. VIRTIS-M measurements were found very sensitive to CO_2 absorption and wing model.

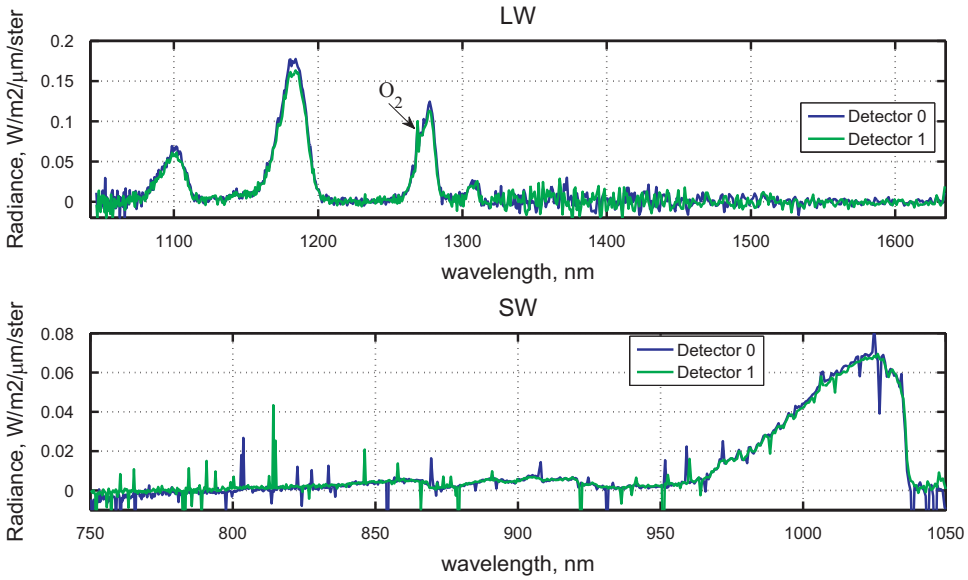

Fig. 18. An example of SPICAV IR nightside observations on orbit 34 with command of "Nadir 1 night". Latitude = 27.01°, longitude = 342.37°, Local time = 2.17 h, emission angle = 33.27°, topography = −0.84 km. The spectra for two detectors are presented for SW and LW channels. 11 spectra have been averaged. The peak of O_2 emission at 1.27 μm is shown.

SPICAV IR allows to measure the H_2O windows with higher spectral resolution providing details of the spectrum sensitive to CO_2 continuum and H_2O mixing ratio, and allowing to test various spectral databases and far wing models (Bézard et al., 2011). Using SPICAV IR in the 1.10- and 1.18-μm windows they inferred water vapor mole fraction of 30^{+10}_{-5} ppm pertaining to the altitude range from 5 to 25 km. The best fit to the measured spectrum is found with an empirical profile reproducing far wing of the $\nu_1+3\nu_3$ ($r=2$) CO_2 band centered at 1206 nm, a composite CO_2 line list combining HITEMP (Pollack et al., 1993), CDSD (Rothman et al., 2010; version from June 2008), BT2 (Barber et al., 2006) databases, and laboratory measurements (Campargue et al., 2010). SPICAV spectra also suggest that the absorption by HDO (new linelists by Voronin et al., 2010) has to be added in the modeling.

Future work with SPICAV H_2O measurements would be to search for possible spatial (or temporal) variations, and explore different elevations to constrain the water vapor profile in the ~0–10 km range, following the method developed by Meadows and Crisp (1996). These measurements may also provide better constraints on the "continuum" opacity allowing to check if it varies quadratically with density as expected for collision-induced bands or far wing opacity.

4.2.4. Oxygen $O_2(a^1\Delta_g)$ and OH nightglows

The O_2 $a^1\Delta$–X3Σ (0–0) band emission at 1.27 μm was first observed on Venus more than 30 years ago (Connes et al., 1979) using Fourier transform spectroscopy from the ground. It is consistent with the excitation scheme of three-body oxygen atoms recombination:

$$O+O+CO_2 \rightarrow O_2^*+CO_2$$

Spatially resolved ground-based observations (Allen et al., 1992; Crisp et al., 1996; Ohtsuki et al., 2008; Bailey et al., 2008a, 2008b) have demonstrated that the distribution of the $O_2(a^1\Delta)$ infrared airglow is variable in space and time. The O_2(a–X) airglow shows regions of enhanced emission which are usually 1000–2000 km wide. Nightside images indicate that these rapidly changing bright areas occur most frequently at low latitudes between midnight and 03:00 local time. During the Galileo flyby of Venus, Drossart et al. (1993) observed with the Near-Infrared Mapping Spectrometer (NIMS) a large enhancement of the 1.27 μm emission near 40°S, over an ~100-km wide area. Many results have been obtained from VIRTIS-M data, mapping the emission from Venus Express. The distribution of the $O_2(a^1\Delta)$ infrared airglow was studied using both nadir and limb viewing geometries. On the limb, Drossart et al. (2007b) determined that the peak of $O_2(a^1\Delta)$ emission profile is located near 96 km. Hueso et al. (2008) used the apparent motion of O_2 (a–X) airglow to track gas masses transported by horizontal winds. This study showed that the pattern changes at some point in 30 min, but large structures usually survive for several hours. Gerard et al. (2008) studied the average $O_2(a^1\Delta)$ infrared nightglow observed with VIRTIS in the southern hemisphere through 11 months of the solar cycle. They found that the brightest emision occurs near the midnight meridian at low latitude. The location of the bright airglow region was further studied by Piccioni et al. (2009) confirming that it is centered on the anti-solar point.

In spite of much larger FOV, the advantage of SPICAV is its relatively high spectral resolution allowing to study the structure of the emission band and to determine the temperature. VIRTIS-M is no longer operational, and SPICAV IR continues to monitor the O_2 emission contributing to the studies of mesospheric dynamics. The example of the O_2 observations at nadir and limb are presented in Fig. 19.

VIRTIS-M data allowed to identify the OH (2–0), (1–0), (2–1) and possibly (3–2) Meinel bands in the Venus limb spectra (Piccioni et al., 2008). The detected limb intensities are 880 ± 90 kiloRayleighs (kR) for the (1–0) band and 100 ± 40 kR for the OH (2–0) band. These emission rates are 55 ± 5 and 480 ± 200 times weaker than the $O_2(a^1\ \Delta)(0–0)$ band intensity at 1.27 μm (Piccioni et al., 2009). The emission layer peaks at an altitude of 96 ± 2 km near midnight. For ten examined orbits, these ratios vary within $\pm 50\%$, but the peak altitude remains constant within the vertical resolution of the measurements. The SPICAV IR has a possibility to monitor the OH 1.43-μm emission at limb, and the appropriate command has been already implemented. Measuring both the O_2 and OH regions would require too long time, and the OH emission is measured by SPICAV separately.

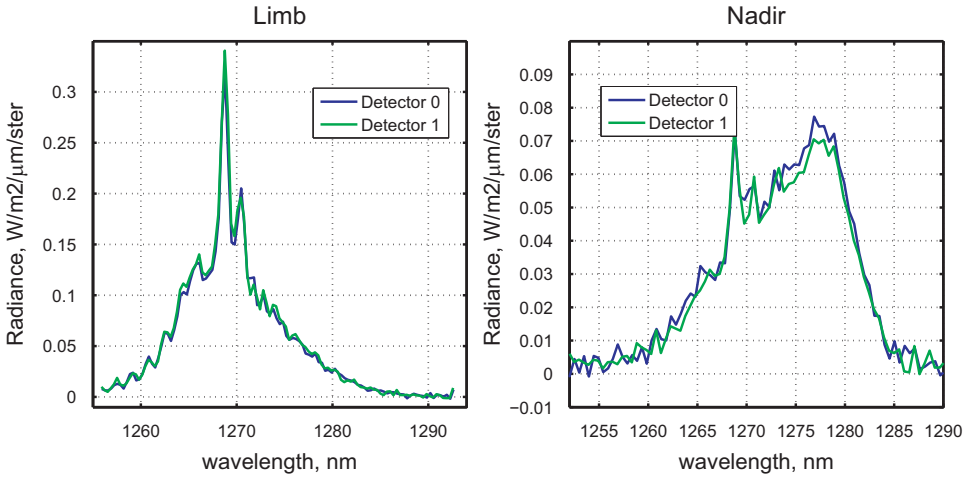

Fig. 19. Examples of the O_2 emission spectra for the nadir and limb measurements. Left: Orbit 1018, limb at altitude 86 km, distance to limb—5000 km, lat.—40°: +30°, longitude—202°, LT=2 h, the 70 spectra have been averaged. Right: Orbit 915, lat. 2.7°, longitude—211°, LT=0.08 h, emission angle=0.02°, topography=0.08 km. 13 spectra have been averaged.

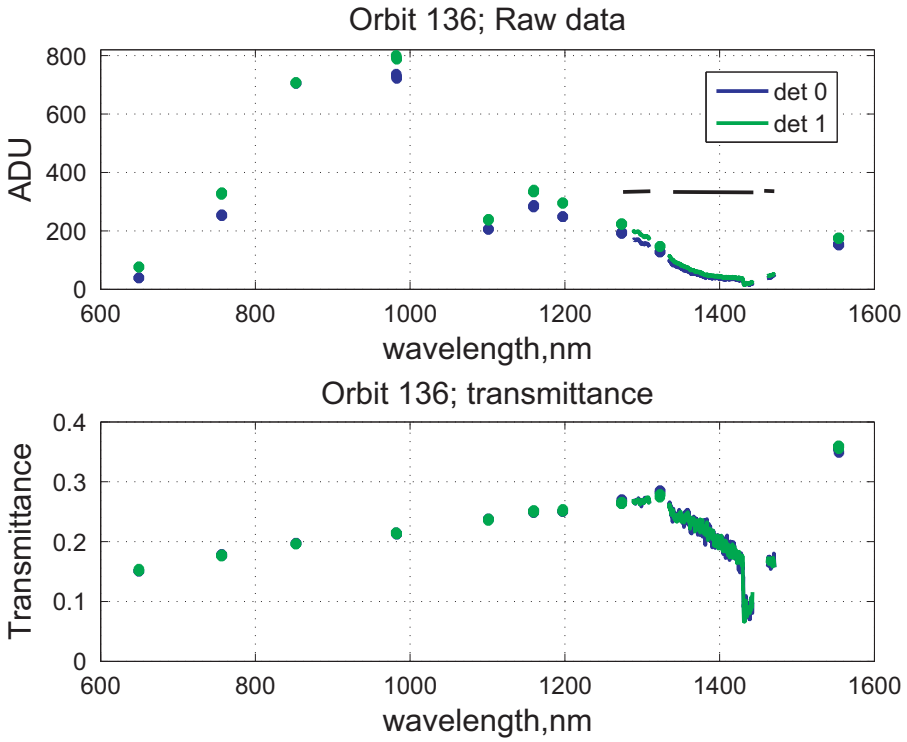

Fig. 20. Solar occultation spectra recorded at Orbit 136 for the command "Sun 1". Top: raw solar spectra for both detectors. Black lines indicate the "windows". Bottom: atmospheric transmittance at altitude of 80 km (latitude 80.1°N; longitude 232.9°, local time 17:08) for both detectors.

4.3. Solar occultations

4.3.1. Operation modes

A special feature of SPICAV/SOIR is its capability to operate in solar occultation mode. Sun occultations are observed simultaneously in the UV and IR (SPICAV+SOIR). Solar occultation is self-calibrated method and does not require any absolute calibrations. The transmittance in the atmosphere can be obtained as the ratio of the observed spectra and the solar spectrum recorded outside the atmosphere. Solar occultations in the IR deliver information about the vertical distribution of aerosols and water vapor. The Sun is a bright source but owing to reduced aperture of the fiber-coupled solar port all the nadir dayside commands can be employed in solar occultations using the sampling time of 2.8 ms. The vertical resolution is determined by the distance to the limb that is highly variable and could be large when observing the southern hemisphere from the apocentre. However, the FOV of the solar port is only 4′, so the resolution on the limb near the pericentre is typically 1–15 km. In turn, higher speed of spacecraft near the pericentre requires to reduce the duration of the spectrum record. Unfortunately, a software problem in the electronic block imposes to use only preprogrammed commands for SPICAV IR in the solar occultation mode, not allowing any optimization in flight. We mostly use a compromise command "Sun 1" with three windows, which include the H_2O and CO_2 bands, and 11 reference wavelengths covering the full spectral range of the spectrometer (Table 3 and Fig. 20). The spectrum takes only 2 s and contains 664 points.

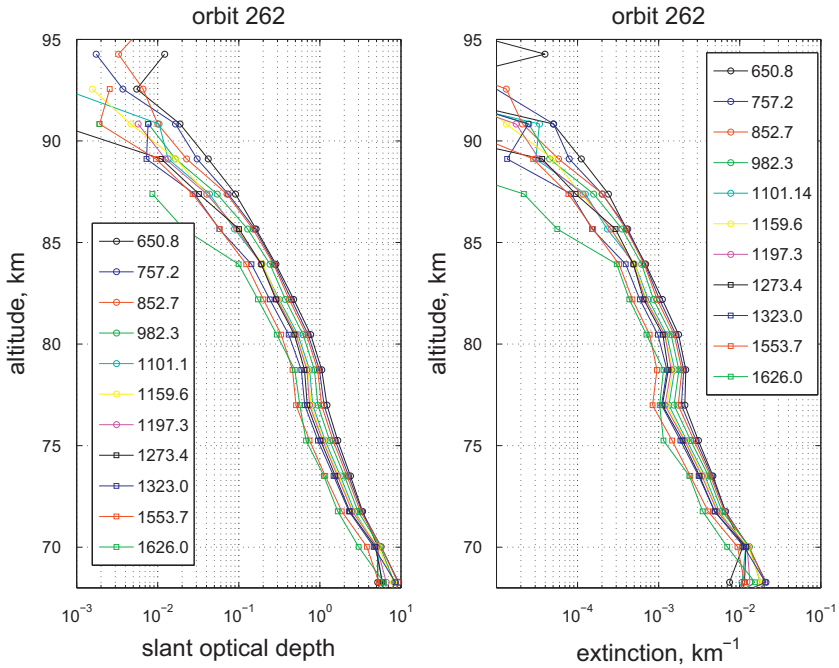

Fig. 21. Vertical profiles of slant optical depth and aerosol extinction obtained for 11 wavelengths (colored numbers in figures) for orbit 262.

The capabilities the AOTF instrument to study the vertical structure of H_2O, CO_2 and aerosol in solar occultation have been successfully demonstrated for the case of Mars (Fedorova et al., 2009; Maltagliati et al., 2011). According to SOIR data the average mixing ratio of H_2O above Venus' clouds (70–110 km) is ~1–2 ppm (Fedorova et al., 2008) that is likely below the detection limit of SPICAV IR. We could not so far retrieve the vertical profiles of water vapor as it was done on Mars, but we used the solar occultation data for aerosol studies.

4.3.2. Vertical profiles of aerosol

Solar occultations give direct information about the opacity on the line of sight. The quality of the IR photometry is good, and the vertical profiles of aerosol extinction at several reference wavelengths are retrieved for all solar occultation sequences in the range of 0.65–1.65 μm (Fig.21). From the opacities the vertical optical depth, particle size and the number density are obtained the high northern latitudes in the altitude range of 65–90 km. Fedorova et al. (2007) has demonstrated that a bimodal distribution (corresponding to aerosol modes 1 and 2 of as detected by Pioneer Venus) was identified for the most of occultations at lower altitudes. Using simultaneous observations by SPICAV UV, IR and SOIR Wilquet et al. (2009) and Montmessin et al. (2008) extended the spectral range from 0.2 to 4 μm and confirm the bi-modal particle size distribution of the Venus upper haze with typical size r_{eff}=0.05 and 0.6 μm.

5. Conclusions

On Venus Express SPICAV IR AOTF spectrometer complements the other channels of SPICAV/SOIR and VIRTIS, filling the gap in spectral range between SPICAV UV and SOIR, and allowing spectral resolution better than VIRTIS-M. It is dedicated to dayside and nightside measurements in nadir, and profiling in solar occultations. SPICAV IR sequentially measures spectra of diffused solar radiation from Venus on the dayside and the emitted Venus radiation in spectral "windows" on the night side and works also in solar occultation mode in the spectral range from 0.65 to 1.7 μm with the resolving power superior to 1500. Sequential registration of the spectrum implies relatively large measurement time, during which the spectrum could change due to the orbital motion. This drawback, to our mind, is compensated by such advantages as flexible sampling within the spectral range, and a very little stray light. As demonstrated with two devices on Mars and Venus Express the AOTF spectrometer is very rugged and stable device suitable for long-term monitoring missions. The mass of the single-pixel spectrometer is only 0.75 kg. On Venus Express some hurried modifications with the spectrometer led to reduced quality of the spectrum in the LW range and in particular of water vapor 1.38-μm band. Nevertheless, it has fully demonstrated the capability of mapping the water vapor both at the dayside and at the nightside, profiling of the aerosols in solar occultation, and sensitivity to detect the O_2 emissions. With VIRTIS M no longer operational this channel remains the only instrument onboard to monitor O_2 emissions and to study the most shortwave near-IR transparency windows.

Acknowledgments

We thank Roscosmos for financing SPICAV in Russia, Russian Academy of Sciences, CNES and CNRS in France, the Belgian government. We wish to thank all our collaborators at the three institutes for the design and fabrication of the instrument (Service d'Aéronomie(LATMOS)/France, BIRA/Belgium and IKI/Moscow). The Russian team acknowledges RFBR grants 10-02-93116, 08-02-01383. We are grateful to Bruno Bézard and Jean-Cloud Gerard for their interest to the instrument and careful calibrations, Sergei Mantsevich for useful discussions on the AOTF. O.Korablev, A.Fedorova and A. Kiselev acknowledge also support from the Russian Government grant to the Moscow Institute of Physics and Technology for the ISPAVR laboratory leading by V.A. Krasnopolsky.

References

Allen, D.A., Crawford, J.W., 1984. Cloud structure on the dark side of Venus. Nature 307, 222–224.

Allen, D., Crisp, D., Meadows, V., 1992. Variable oxygen airglow on Venus as a probe of atmospheric dynamics. Nature 359 (6395), 516–519.

Bailey, J., Meadows, V.S., Chamberlain, S., Crisp, D., 2008a. The temperature of the Venus mesosphere from O_2 ($a\Delta g1$) airglow observations. Icarus 197 (1), 247–259.

Bailey, J., Chamberlain, S., Crisp, D., Meadows, V.S., 2008b. Near infrared imaging spectroscopy of Venus with the Anglo-Australian Telescope. Planetary and Space Science 56 (10), 1385–1390.

Baines, K.H., Bellucci, G., Bibring, J.-P., Brown, R.H., Buratti, B.J., Bussoletti, E., Capaccioni, F., Cerroni, P., Clark, R.N., Coradini, A., Cruikshank, D.P., Drossart, P., Formisano, V., Jaumann, R., Langevin, Y., Matson, D.L., McCord, T.B., Mennella, V., Nelson, Robert, M., Nicholson, P.D., Sicardy, B., Sotin, C., Hansen, G.B., Aiello, J.J., Amici, S, 2000. Detection of sub-micron radiation from the surface of Venus by Cassini/VIMS. Icarus 148 (1), 307–311.

Barber, R.J., Tennyson, J., Harris, G.J., Tolchenov, R.N., 2006. A high-accuracy computed water line list. Monthly Notices of the Royal Astronomical Society 368, 1087–1094.

Belyaev, D., Korablev, O., Fedorova, A., Bertaux, J.-L., Vandaele, A.C., Montmessin, F., Mahieux, A., Wilquet, V., Drummond, R., 2008. First observations of SO_2 above Venus' clouds by means of solar occultation in the infrared. Journal of Geophysical Research 113 (2). doi:10.1029/2008JE003143. CiteID E00B25.

Belyaev, D., Montmessin, F., Bertaux, J.-L., Mahieux, A., Fedorova, A., Korablev, O., Marcq, E., Yung, Y.-L., Zhang, X., 2012. Vertical profiling of SO_2 and SO above Venus' clouds by SPICAV/SOIR solar occultations. Icarus 217, 740–751.

Bertaux, J.-L., Korablev, O., Perrier, S., Quémerais, E., Montmessin, F., Leblanc, F., Lebonnois, S., Lefèvre, F., Forget, F., Fedorova, A., Rannou, P., Dimarellis, E., Reberac, A., Fonteyn, D., Chaufray, J.Y., Guibert, S., 2006. SPICAM on Mars Express: observing modes and overview of UV Spectrometer data and scientific results. Journal of Geophysical Research 111, E10S90. doi:10.1029/2006JE002690.

Bertaux, J.-L., Nevejans, D., Korablev, O., Villard, E., Quemerais, E., Neefs, E., Montmessin, F., Leblanc, F., Dubois, J.-P., Dimarellis, E., Hauchecorne, A., Lefevre, F., Rannou, P., Chaufray, J.Y., Cabane, M., Cernogora, G., Souchon, G., Semelin, F., Reberac, A., Van Ransbeeck, E., Berkenbosch, S., Clairquin, R., Muller, C., Forget, F., Hourdin, F., Talagrand, O., Rodin, A., Fedorova, A., Stepanov, A., Vinogradov, I., Kiselev, A., Kalinnikov, Y., Durry, G., Sandel, B.R., Stern, A., Gerard, J.-C., 2007a. SPICAV on Venus Express: three spectrometers to study the global structure and composition of the Venus atmosphere. Planetary and Space Science 55, 1673–1700.

Bertaux, J.-L., Vandaele, A.-C., Korablev, O., Villard, E., Fedorova, A., Fussen, D., Quémerais, E., Beliaev, D., Mahieux, A., Montmessin, F., Müller, C., Neefs, E., Nevejans, D., Wilquet, V., Dubois, J.-P., Hauchecorne, A., Stepanov, A., Vinogradov, A., Rodin, A., 2007b. A warm layer in Venus' cryosphere and high altitude measurements of HF, HCl, H_2O and HDO. Nature 450, 646–649.

Bézard, B., de Bergh, C., Crisp, D., Maillard, J.-P., 1990. The deep atmosphere of Venus revealed by high-resolution nightside spectra. Nature 345, 508–511.

Bézard, B., Tsang, C.C.C., Carlson, R.W., Piccioni, G., Marcq, E., Drossart, P., 2009. Water vapor abundance near the surface of Venus from Venus Express/VIRTIS observations. Journal of Geophysical Research 114, E00B39. doi:10.1029/2008JE003251.

Bézard, B., Fedorova, A., Bertaux, J.-L., Rodin, A., Korablev, O., 2011. The 1.10- and 1.18-μm nightside windows of Venus observed by SPICAV-IR aboard Venus Express. Icarus 216, 173–183.

Campargue, A., Song, K.F., Mouton, N., Perevalov, V.I., Kassi, S., 2010. High sensitivity CW-Cavity Ring Down Spectroscopy of five $^{13}CO_2$ isotopologues of carbon dioxide in the 1.26–1.44 μm region (I): Line positions. Journal of Quantitative Spectroscopy and Radiative Transfer 111, 659–674.

Cardesín, M.A., Piccioni, G., Ammannito, E., Filacchione, G., Drossart, P., 2010. Calibration of hyperspectral imaging data: VIRTIS-M Onboard Venus Express. IEEE Transactions on Geoscience and Remote Sensing 48, 3941–3950.

Connes, P., Noxon, J.F., Traub, W.A., Carleton, N.P., 1979. O2/1 Delta/ emission in the day and night airglow of Venus. Astrophysical Journal 233, L29–L32.

Cottini, V., Ignatiev, N.I., Piccioni, G., Drossart, P., Grassi, D., Markiewicz, W.J., 2012. Mesospheric water vapor on Venus from Venus-Express/VIRTIS dayside data. Icarus 217, 561–569.

Crisp, D., Allen, D.A., Grinspoon, D.H., Pollack, J.B., 1991. The dark side of Venus—near-infrared images and spectra from the Anglo-Australian Observatory. Science 253, 1263–1266.

Crisp, D., Meadows, V.S., Bézard, B., de Bergh, C., Maillard, J.-P., Mills, F.P., 1996. Ground-based near-infrared observations of the Venus nightside: 1.27-μm $O_2(a\Delta_g)$ airglow from the upper atmosphere. Journal of Geophysical Research 101 (E2), 4577–4594.

Drossart, P., Bézard, B., Encrenaz, Th., Lellouch, E., Roos, M., Taylor, F.W., Collard, A.D., Calcutt, S.B., Pollack, J., Grinspoon, D.H., 1993. Search for spatial variations of the H_2O abundance in the lower atmosphere of Venus from NIMS-Galileo. Planetary and Space Science 41 (7), 495–504.

Drossart, P., Piccioni, G., Adriani, A., Angrilli, F., Arnold, G., Baines, K.H., Bellucci, G., Benkhoff, J., Bézard, B., Bibring, J.-P., Blanco, A., Blecka, M.I., Carlson, R.W., Coradini, A., di Lellis, A., Encrenaz, T., Erard, S., Fonti, S., Formisano, V., Fouchet, T., Garcia, R., Haus, R., Helbert, J., Ignatiev, N.I., Irwin, P.G.J., Langevin, Y., Lebonnois, S., Lopez-Valverde, M.A., Luz, D., Marinangeli, L., Orofino, V., Rodin, A.V., Roos-Serote, M.C., Saggin, B., Sanchez-Lavega, A., Stam, D.M., Taylor, F.W., Titov, D., Visconti, G., Zambelli, M., Hueso, R., Tsang, C.C.C., Wilson, C.F., Afanasenko, T.Z., 2007a. Scientific goals for the observation of Venus by VIRTIS on ESA/Venus express mission. Planetary and Space Science 55 (12), 1653–1672.

Drossart, P., Piccioni, G., Gérard, J.C., Lopez-Valverde, M.A., Sanchez-Lavega, A., Zasova, L., Hueso, R., Taylor, F.W., Bézard, B., Adriani, A., 2007b. A dynamic upper atmosphere of Venus as revealed by VIRTIS on Venus Express. Nature 450 (7170), 641–645.

Epikhin, V.M., Vizen, F.L., Pustovoit, V.I., 1984. Acousto-optic filter. Pat. Russia #1247816, 22.10.1984.

Evans, K.F., 1998. The spherical harmonics discrete ordinate method for three-dimensional atmospheric radiative transfer. Journal of the Atmospheric Science 55, 429–446.

Fedorova, A., Korablev, O., Bertaux, J.-L., Rodin, A., Kiselev, A., Perrier, S., 2006. Mars water vapor abundance from SPICAM IR spectrometer: seasonal and geographic distributions. Journal of Geophysical Research 111, E09S08. doi:10.1029/2006JE002695.

Fedorova, A., Korablev, O., Bertaux, J.-L., Belyaev, D., Villard, E., Nevejans, D., Vandaele, A.-C., Neefs, E., Wilquet, V., 2007. The Venus upper haze from SPICAV/SOIR infrared experiments on Venus-Express. EGU2007-A-09742.

Fedorova, A., Korablev, O., Vandaele, A.C., Bertaux, J.-L., Belyaev, D., Mahieux, A., Neefs, E., Wilquet, V., Drummond, R., Montmessin, F., Villard, E., 2008. HDO and H_2O vertical distributions and isotopic ratio in the Venus mesosphere by SOIR spectrometer on board Venus-Express. Journal of Geophysical Research 113, E12. doi:10.1029/2008JE003146. CiteID E00B22.

Fedorova, A., Korablev, O., Bertaux, J.-L., Rodin, A., Montmessin, F., Belyaev, D., Reberac, A., 2009. Solar infrared occultations by the SPICAM Experiment on Mars-Express: simultaneous observations of H_2O, CO_2 and aerosol vertical distribution. Icarus 200 (1), 96–117.

Fedorova, A., Korablev, O., Bertaux, J.-L., Montmessin, F., Belyaev, D., Mahieux, A., Vandaele, A.C., 2010. Water vapor distribution in the Venusian mesosphere from SPICAV/SOIR observations. In: 38th COSPAR Scientific Assembly 2010, C31-0011-10.

Gérard, J.-C., Saglam, A., Piccioni, G., Drossart, P., Cox, C., Erard, S., Hueso, R., Sánchez-Lavega, A., 2008. Distribution of the O_2 infrared nightglow observed with VIRTIS on board Venus Express. Geophysical Research Letters 35 (2). CiteID L02207.

Hashimoto, G.L., Sugita, S., 2003. On observing the compositional variability of the surface of Venus using nightside near-infrared thermal radiation. Journal of Geophysical Research 108 (E9), 1–13. doi:10.1029/2003JE002082. CiteID 5109.

Hueso, R., Sánchez-Lavega, A., Piccioni, G., Drossart, P., Gérard, J.C., Khatuntsev, I., Zasova, L., Migliorini, A., 2008. Morphology and dynamics of Venus oxygen airglow from Venus Express/Visible and Infrared Thermal Imaging Spectrometer observations. Journal of Geophysical Research, 113. CiteID E00B02.

Ignatiev, N.I., Moroz, V.I., Moshkin, B.E., Ekonomov, A.P., Gnedykh, V.I., Grigoriev, A.V., Khatuntsev, I.V., 1997. Water vapour in the lower atmosphere of Venus: a new analysis of optical spectra measured by entry probes. Planetary and Space Science 45, 427–438.

Ignatiev, N.I., Moroz, V.I., Zasova, L.V., Khatuntsev, I.V., 1999. Water vapour in the middle atmosphere of Venus: an improved treatment of the Venera 15 IR spectra. Planetary and Space Science 47 (8–9), 1061–1075.

Ignatiev, N.I., Titov, D.V., Piccioni, G., Drossart, P., Markiewicz, W.J., Cottini, V., Roatsch, Th., Almeida, M., Manoel, N., 2009. Altimetry of the Venus cloud tops from the Venus Express observations. Journal of Geophysical Research 114 (E5). CiteID E00B43.

Kawabata, K., Coffeen, D.L., Hansen, J.E., Lane, W.A., Sato, M., Travis, L.D., 1980. Cloud and haze properties from pioneer Venus polarimetry. Journal of Geophysical Research 85, 8129–8140.

Keating, G.M., Bertaux, J.-L., Bougher, S.W., Cravens, T.E., Dickinson, R.E., Hedin, A.E., Krasnopolsky, V.A., Nagy, A.F., Nicholson, J.Y., Paxton, L.J., Von Zahn, U., 1985. VIRA (Venus International Reference Atmosphere). In: Kliore, A.J., Moroz, V.I., Keating, G.M. (Eds.), Models of Venus neutral upper atmosphere: structure and composition. Advances in Space Research 5(11), 117–171.

Korablev, O., Bertaux, J-L., Grigoriev, A., Dimarellis, E., Kalinnikov, Yu., Rodin, A., Muller, C., Fonteyn, D., 2002a. An AOTF-based spectrometer for the studies of Mars atmosphere for Mars Express mission. Advances in Space Research 29 (2), 143–150.

Korablev, O.I., Bertaux, J.L., Dimarellis, E., Grigoriev, A., Kalinnikov, Yu., Stepanov, A., Guibert, S., 2002b. AOTF-based spectrometer for Mars atmosphere sounding. In: Strojnik, M., Andresen, B.F. (Ed.), Infrared Spaceborne Remote Sensing, vol. X. SPIE. Proceedings of SPIE 4818, 261–271.

Korablev, O., Bertaux, J.-L., Fedorova, A., Fonteyn, D., Stepanov, A., Kalinnikov, Yu., Kiselev, A., Grigoriev, A., Jegoulev, V., Perrier, S., Dimarellis, E., Dubois, J.-P., Reberac, A., Van Ransbeeck, E., Gondet, B., Montmessin, F., Rodin, A., 2006. SPICAM IR acousto-optic spectrometer experiment on Mars Express. Journal of Geophysical Research 111, E09S03. doi:10.1029/2006JE002696. [Paper I].

Koukouli, M.E., Irwin, P.G.J., Taylor, R.W., 2005. Water vapor abundance in Venus' middle atmosphere from Pioneer Venus OIR and Venera 15 FTS measurements. Icarus 173, 84–99.

Kurucz, R., 1995. The solar spectrum: atlases and line identifications. In: Saival, A.J. Blomme, R., Grevesse, N. (Eds.), Workshop on Laboratory and Astronomical High Resolution Spectra, Astronomical Society of the Pacific (ASP) Conference Series, Proceeding of ASP Conference, vol. 81, Brussles, Belgium, 29 August–2 September 1994, San Francisco, p. 17.

Mahieux, A., Berkenbosh, S., Clairquin, R., Fussen, D., Mateshvili, N., Neefs, E., Nevejans, D., Ristic, B., Vandaele, A.C., Wilquet, V., Belyaev, D., Fedorova, A., Korablev, O., Bertaux, J.L., 2008. In-Flight performance and calibration of SPICAV SOIR on board Venus Express. Applied Optics 47, 2252–2265.

Maltagliati, L., Montmessin, F., Fedorova, A., Korablev, O., Forget, F., Bertaux, J.-L., 2011. Evidence of water vapor in excess of saturation in the atmosphere of Mars. Science 333, 1868–1871.

Marcq, E., Bézard, B., Drossart, P., Piccioni, G., Reess, J.M., Henry, F., 2008. A latitudinal survey of CO, OCS, H_2O, and SO_2 in the lower atmosphere of Venus: spectroscopic studies using VIRTIS-H. Journal of Geophysical Research, 113. CiteID E00B07.

Marcq, E., Belyaev, D., Montmessin, F., Fedorova, A., Bertaux, J.-L., Vandaele, A.-C., Neefs, E., 2011. An investigation of the SO_2 content of the Venusian Mesosphere using SPICAV-UV in Nadir mode. Icarus 211 (1), 58–69. doi:10.1016/j.icarus.2010.08.021.

Meadows, V.S., Crisp, D., 1996. Ground-based near-infrared observations of the Venus nightside: the thermal structure and water abundance near the surface. Journal of Geophysical Research 101 (E2), 4595–4622.

Montmessin, F., Fedorova, A., Wilquet, V., Mahieux, A., Drummond, R., Korablev, O., Vandaele, A., Bertaux, J.-L., 2008. Venusian upper haze properties: detection of a multimodal distribution at high altitude by SPICAV/SOIR. American Geophysical Union, Fall Meeting 2008, abstract #P33A-1428.

Moroz, V.I., 1981. The albedo of Venus in the range 0.2–4.0 μm. Kosmicheskie Issledovaniia 19, 591–598.

Nevejans, D., Neefs, E., Van Ransbeeck, E., Berkenbosch, S., Clairquin, R., De Vos, L., Moelans, W., Glorieux, S., Baeke, A., Korablev, O., Vinogradov, I., Kalinnikov, Y., Bach, B., Dubois, J.-P., Villard, E., 2006. Compact high-resolution space-borne echelle grating spectrometer with AOTF based order sorting for the infrared domain from 2.2 to 4.3 μm. Applied Optics 45 (21), 5191–5206.

Ohtsuki, S., Iwagami, N., Sagawa, H., Ueno, M., Kasaba, Y., Imamura, T., Yanagisawa, K., Nishihara, E., 2008. Distributions of the Venus 1.27-μm O_2 airglow and rotational temperature. Planetary and Space Science 56 (10), 1391–1398.

Piccioni, G., Drossart, P., Zasova, L., Migliorini, A., Gérard, J.-C., Mills, F.P., Shakun, A., García Muñoz, A., Ignatiev, N., Grassi, D., Cottini, V., Taylor, F.W., Erard, S., 2008. First detection of hydroxyl in the atmosphere of Venus. Astronomy and Astrophysics 483 (3), L29–L33.

Piccioni, G., Zasova, L., Migliorini, A., Drossart, P., Shakun, A., García Muñoz, A., Mills, F.P., Cardesin-Moinelo, A., 2009. Near-IR oxygen nightglow observed by VIRTIS in the Venus upper atmosphere. Journal of Geophysical Research, 114. CiteID E00B38.

Pollack, J.B., Dalton, J.B., Grinspoon, D., Wattson, R.B., Freedman, R., Crisp, D., Allen, D.A., Bézard, B., de Bergh, C., Giver, L.P., Ma, Q., Tipping, R., 1993. Near-infrared light from Venus' nightside—a spectroscopic analysis. Icarus 103 (1), 1–42.

Rothman, L.S., Gordon, I.E., Barbe, A., Benner, D.C., Bernath, P.F., Birk, M., et al., 2009. The HITRAN 2008 molecular spectroscopic database. JQSRT 110, 533–572.

Rothman, L.S., Gordon, I.E., Barber, R.J., Dothe, H., Gamache, R.R., Goldman, A., Perevalov, V.I., Taschkun, S.A., Tennyson, J., 2010. HITEMP, the high-temperature molecular spectroscopic database. Journal of Quantitative Spectroscopy and Radiative Transfer 111, 2139–2150.

Sandor, B.J., Clancy, R.T., 2005. Water vapor variations in the Venus mesosphere from microwave spectra. Icarus 177 (1), 129–143.

Sato, M., Travis, L.D., Kawabata, K., 1996. Photopolarimetry analysis of the Venus atmosphere in polar regions. Icarus 124 (2), 569–585.

Svedhem, H., Titov, D.V., McCoy, D., Lebreton, J.–P., Barabash, S., Bertaux, J.–L., Drossart, P., Formisano, V., Häusler, B., Korablev, O., Markiewicz, W.J., Nevejans, D., Pätzold, M., Piccioni, G., Zhang, T.L., Taylor, F.W., Lellouch, E., Koschny, D., Witasse, O., Eggel, H., Warhaut, M., Accomazzo, A., Rodriguez-Canabal, J., Fabrega, J., Schirmann, T., Clochet, A., Coradini, M., 2007. Venus Express—the first European mission to Venus. Planetary and Space Science 55, 1636–1652.

Svedhem, H., Titov, D., Taylor, F., Witasse, O., 2009. Venus Express mission. Journal of Geophysical Research, 114. E00B33–+.

Thuillier, G., Hersé, M., Labs, D., Foujols, T., Peetermans, W., Gillotay, D., Simon, P.C., Mandel, H., 2003. The solar spectral irradiance from 200 to 2400 nm as measured by the SOLSPEC spectrometer from the Atlas and Eureca missions. Solar Physics 214 (1), 1–22.

Titov, D.V., et al., 2006. Venus Express science planning. Planetary and Space Science 54, 1279–1297.

Tsang, C.C.C., Irwin, P.G.J., Wilson, C.F., Taylor, F.W., Lee, C., de Kok, R., Drossart, P., Piccioni, G., Bézard, B., Calcutt, S., 2008. Tropospheric carbon monoxide concentrations and variability on Venus from Venus Express/VIRTIS-M observations. Journal of Geophysical Research 113 (7). CiteID E00B08.

Vandaele, A.C., De Maziere, M., Drummond, R., Mahieux, A., Neefs, E., Wilquet, V., Korablev, O., Fedorova, A., Belyaev, D., Montmessin, F., Bertaux, J.-L., 2008. Composition of the Venus mesosphere measured by Solar Occultation at Infrared on board Venus Express. Journal of Geophysical Research 113, E13. doi:10.1029/2008JE003140. CiteID E00B23.

Voronin, B.A., Tennyson, J., Tolchenov, R.N., Lugovskoy, A.A., Yurchenko, S.N., 2010. A high accuracy computed line list for the HDO molecule. Monthly Notices of the Royal Astronomical Society 402, 492–496.

Wilquet, V., Fedorova, A., Montmessin, F., Drummond, R., Mahieux, A., Vandaele, A.-C., Villard, E., Korablev, O., Bertaux, J.-L., 2009. Preliminary characterization of the upper haze by SPICAV/SOIR solar occultation in UV to mid-IR onboard Venus Express. Journal of Geophysical Research 114, E00B42. doi:10.1029/2008JE003186.

Wilson, C.F., Tsang, C.C.C., Irwin, P.G.J., Taylor, F.W., Bézard, B., Erard, S., Carlson, R.W., Drossart, P., Piccioni, G., Holmes, R.C., 2009. Analysis of thermal emission from the nightside of Venus at 1.51 and 1.55 μm. Icarus 201, 814–817.